Some pluripotency-related genes, including *Nanog*, *Oct3/4*, and *Lin28a*, were upregulated in the Dox-withdrawn kidney tumor cells as compared to normal kidney tissue, although the expression levels of both *Nanog* and endogenous *Oct3/4* were significantly lower than that of pluripotent stem cells (Figures 3C and S3C). Conversely, other pluripotency-related genes, such as *Esrrb*, were not upregulated in these tumors (Figures 3C).

To further characterize Dox-withdrawn tumor cells, we sought to identify tumor-cell-specific markers. We found that *Lgr5* is specifically upregulated in Dox-withdrawn kidney tumor cells, but not in adult kidney tissues or pluripotent stem cells (Figure 3D). Increased expression of *Lgr5* was similarly observed in the transplanted secondary tumors (Figure S3D). Therefore, we established iPSC lines from OSKM-inducible MEFs containing *Lgr5-EGFP* reporter allele in which *Lgr5* expression can be visualized by enhanced green fluorescent protein (EGFP) (Barker et al., 2007). The established *Lgr5*-reporter iPSCs do not express EGFP in ESC culture conditions (Figure S3E). OSKM-inducible *Lgr5* reporter chimeric mice at 4 weeks of age were treated with the 7+/7− Dox regimen. Again, these mice developed Dox-withdrawn kidney tumors consisting of dysplastic cells (Figure 3E). The scattered EGFP signals were observed in kidney tumors (Figure 3E), and immunohistochemical analysis revealed that *Lgr5* is specifically expressed in part of Dox-withdrawn kidney tumor cells (Figures 3E and S3E). These findings indicate that Dox-withdrawn kidney tumors contain *Lgr5*-positive cells and that the *Lgr5* reporter allele is available to specifically identify the Dox-withdrawn kidney tumor cells that are distinct from fully reprogrammed pluripotent stem cells. Of note, some of the *Lgr5*-expressing tumor cells also expressed Oct3/4 and Lin28b in immunohistochemical analysis (Figures 3F and S3F), thus suggesting that *Lgr5*-expressing tumor cells share some characteristics with pluripotent stem cells. The fact that Dox treatment for longer than 8 days followed by Dox withdrawal often results in teratoma formation supports the notion that partial reprogramming toward pluripotent stem cells is involved in the development of Dox-withdrawn tumors (data not shown). Altogether, our findings indicate that *Lgr5*-expressing tumor cells are distinct from pluripotent stem cells but contain partially reprogrammed cells.

Failed Repression of ESC-Polycomb Targets in Dox-Withdrawn Tumors

In contrast to ESC-like activation observed for both the ESC-Core and ESC-Myc modules, the ESC Polycomb repressive complex (PRC) module was differentially expressed between Dox-withdrawn tumors and ESCs (Figure 4A). We found that a number of ESC-PRC targeted genes are not repressed in both kidney tumors and transplanted secondary tumors (Figures 4A, S4A, and S4B), indicating that the failed repression of ESC-PRC targets is associated with the development of Dox-withdrawn tumors. Consistent with the notion, more than one-forth of the upregulated genes in tumor cells as compared to ESCs (greater than 3-fold upregulation) were targets of PRC in ESCs (Mikkelsen et al., 2007) (Table S1). We also found that Dox-withdrawn kidney tumors express kidney-precursor-expressing genes such as *Six2*, *Eya1*, and *Lgr5* (Barker et al., 2012; Kobayashi et al., 2008) (Figures 4B and S4C). In particular, *Six2* and *Lgr5*, which are also PRC targets in ESCs (Mikkelsen et al., 2007), are specifically upregulated in both Dox-withdrawn kidney tumors and secondary tumors when compared to both normal kidney tissues and pluripotent stem cells (Figures 3D, 4B, S3D, and S4D). Chromatin immunoprecipitation (ChIP)-qPCR experiments confirmed decreased H3K27me3 levels at both *Six2* and *Lgr5* promoter regions in Dox-withdrawn tumors when compared with those in normal kidney tissues (Figure S4E). Failed repression of the ESC-PRC module was also detectable in unsuccessfully reprogrammed kidney cells in vitro, which were established by the transient expression of reprogramming factors in isolated kidney tubule cells in vitro (Figure S4F).

We next examined the kinetics of transcriptional changes during the development of the Dox-withdrawn tumors. Immunohistochemical analysis revealed that early dysplastic cells at day 7 coincide with transgene-expressing cells (Figure S4G). Taking advantage of florescence-linked transgene expression in our mice, we fluorescence-activated cell sorted mCherry-positive kidney cells in OSKM mice given Dox for 7 days (D7), isolating early dysplastic cells for gene expression analysis. Fluorescence-activated cell-sorted D7 LacZ-mCherry-expressing kidney cells were used as a control (Figure S4H). Decreased expression of proximal tubule cell markers was observed in the D7 OSKM cells as compared to D7 LacZ cells, suggesting that the loss of kidney cell identity occurs in early dysplastic cells (Figure S4I). In contrast, increased expression of ectopic stem/progenitor cell markers was not evident in D7 OSKM cells (Figure S4I). These findings suggest that remodeling of global transcriptional profiles toward a stem/progenitor-like state is specifically associated with transgene-independent, late dysplastic cells.

To investigate cell-of-origin effects on failed reprogramming, we next performed a microarray analysis for Dox-withdrawn liver tumors and compared the data with that of kidney tumors. As observed in kidney tumors, the liver tumors displayed failed repression of the ESC-PRC module, accompanied by activation of both the ESC-Core and Myc modules (Figure S4J; Table S1). Although derepressed PRC module genes in kidney tumors and liver tumors often overlapped (Figure S5A; Table S1), we found differentially derepressed PRC genes between kidney and liver tumors. Notably, such differentially derepressed PRC genes were associated with kidney and liver development, respectively. These findings suggest that failed PRC repression in Dox-withdrawn tumors may be associated with the activation of a developmental transcription

(F) Dox-withdrawn tumors express pluripotency-related proteins. Double immunofluorescence for Lin28b and GFP (Lgr5) revealed that the GFP-positive tumor cells also expressed Lin28b. Double immunofluorescence for Oct3/4 and GFP (Lgr5) showed that a subset of GFP-positive tumor cells expressed Oct3/4 in the nucleus. Scale bars, 20 μm.
See also Figure S3.

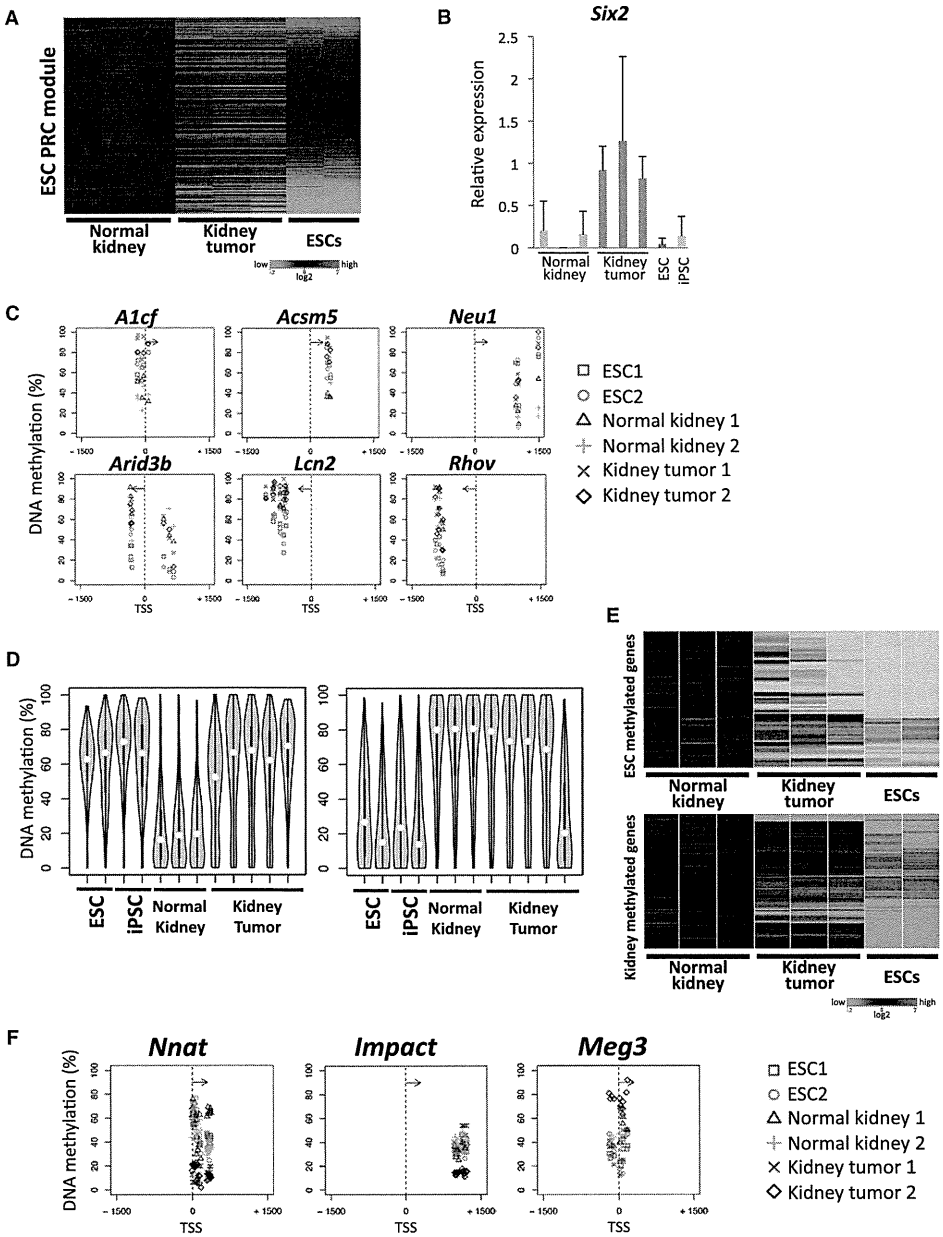

Figure 4. Altered Epigenetic Regulation in Dox-Withdrawn Tumors

(A) The microarray analyses revealed that ESC-PRC target genes were often activated in Dox-withdrawn kidney tumors compared to normal kidney tissues.

(B) *Six2* was highly expressed only in the Dox-withdrawn kidney tumors. Data are presented as mean ± SD. The mean level of kidney tumors was set to 1.

(C) Altered DNA methylation patterns in Dox-withdrawn tumors and the DNA methylation status of representative genes in the RRBS analyses.

(D) The global analyses for the DNA methylation levels. Genes that were differentially methylated between ESCs and normal kidney samples (more than 30% difference) were extracted and then analyzed for DNA methylation levels in Dox-withdrawn kidney tumors. Kidney tumors gain DNA methylation at ESC-methylated genes, whereas kidney-methylated genes often retain their methylation status in kidney tumors.

(legend continued on next page)

program, which is affected in part by the cell of origin (Figure S5A).

Altered DNA Methylation in Dox-Withdrawn Kidney Tumor Cells

Somatic cell reprogramming is accompanied by global changes in DNA methylation patterns (Mikkelsen et al., 2008). The fact that failed reprogramming can cause tumor development suggests that altered epigenetic modifications play a role in tumorigenesis. To quantitatively profile DNA methylation in Dox-withdrawn tumors, we next performed reduced representation bisulfite sequencing (RRBS) (Meissner et al., 2005). We identified a number of genes with altered DNA methylation levels in Dox-withdrawn tumors as compared to normal kidney tissues. Dox-withdrawn tumors revealed frequent gains of DNA methylation at DNA-methylated genes in ESCs, whereas loss of methylation at DNA-methylated genes in kidney tissues was not evident (Figure 4C). To validate these findings, we next performed a global analysis. We first extracted genes differentially methylated between ESCs and normal kidney samples and then examined their DNA methylation in Dox-withdrawn tumors. The global analysis confirmed that Dox-withdrawn kidney tumors gained de novo methylation at ESC-methylated genes, whereas kidney-methylated genes often retain their methylation in Dox-withdrawn kidney tumors (Figure 4D). Consistent with these findings, ESC-methylated genes were frequently found to be repressed in Dox-withdrawn tumors, whereas kidney-methylated genes tended to remain silent in these tumors (Figure 4E). These results suggest that loss of somatic cell-specific DNA methylation is preceded by a gain of ESC-specific DNA methylation patterns during the reprogramming process.

Adult cancers generally exhibit two distinct patterns of alterations in DNA methylation: site-specific DNA hypermethylation and global DNA hypomethylation (Jones and Baylin, 2002; Yamada et al., 2005). We performed specified regional analyses for the DNA methylation in normal kidney tissues and Dox-withdrawn kidney tumors. DNA hypermethylation at promoter regions in Dox-withdrawn tumors was not detectable, regardless of the presence of CpG islands (Figure S5B). Additionally, decreased DNA methylation levels at intergenic regions were not obvious in Dox-withdrawn tumors (Figure S5B).

We found that Dox-withdrawn kidney tumors aberrantly express a number of imprinted genes and that altered expression levels are similar to those in ESCs (Figure S5C). When DNA methylation status at differentially methylated regions (DMRs) of imprinted genes were examined in Dox-withdrawn tumors using a MassARRAY platform (Ehrich et al., 2005), we found frequent alterations of DNA methylation status at DMRs in Dox-withdrawn tumors (Figure S5D). The aberrant genomic methylation levels at imprinted genes in Dox-withdrawn tumors were also confirmed by RRBS analysis (Figures 4F and S5E). Intriguingly, each Dox-withdrawn tumor revealed variable aberrations in DNA methylation at different imprinted genes. The aberrant methylation includes hypermethylation at the *Meg3* (*Gtl2*) DMR, which has been correlated with impaired differentiation properties of iPSCs (Stadtfeld et al., 2010a) (Figures 4F and S5E). Moreover, SNP analysis in the hybrid KH2 background revealed that the altered expression of some imprinted genes in Dox-withdrawn tumors arise from biallelic transcription, compared to monoallelic expression in the original OSKM-inducible ESCs (Figure S5F). Collectively, these results suggest that genomic imprinting is unstable in Dox-withdrawn tumors and provide additional evidence that altered gene expression underlying tumor development is associated with altered epigenetic signatures.

Dox-Withdrawn Kidney Tumors Resemble Wilms Tumors

Histological analysis revealed that Dox-withdrawn kidney tumors in reprogrammable mice resemble Wilms tumor, the most common pediatric kidney cancer (Figure 5A). A number of studies demonstrated that increased expression of *Igf2* with DNA hypermethylation at the *H19* DMR is one of the causative and most common alterations in Wilms tumors (Ogawa et al., 1993; Steenman et al., 1994). We confirmed that Dox-withdrawn tumors express a significantly higher level of *Igf2* than noninduced tissues (Figures 5B and S6A). Moreover, consistent with altered DNA methylation at other imprinted genes, the increased methylation at the *H19* DMR was detectable in some Dox-withdrawn kidney tumors (Figure 5C).

To additionally evaluate the similarity between Dox-withdrawn kidney tumors and Wilms tumors, we next compared global gene expression patterns. We first selected genes that are upregulated more than 5-fold in Dox-withdrawn kidney tumors in comparison with noninduced kidney tissues and then assessed expression of their human orthologs in human normal kidney tissues, Wilms tumors, and human ESCs (hESCs) using previously reported microarray data sets (Tchieu et al., 2010; Yusenko et al., 2009). We found that upregulated genes in Dox-withdrawn kidney tumors are frequently upregulated in both Wilms tumors and hESCs as compared to normal kidney samples (Figure 5D), whereas this upregulation is not evident in adult kidney cancers (renal cell carcinomas [RCCs]) (Figure S6B).

We also analyzed the expression of genes in ESC-Core, ESC-Myc, and ESC-PRC modules in Wilms tumors. Notably, ESC-upregulated genes in both ESC-Core and ESC-Myc modules are similarly activated in Wilms tumors (Figures 5D and S6C), although *NANOG* and *OCT3/4* are not expressed in Wilms tumors. In contrast, a fraction of ESC-PRC targeted genes expressed in kidney progenitors, such as *SIX2* and *LGR5*, are specifically upregulated in Wilms tumors as compared with

(E) DNA-methylation-associated gene regulation in Dox-withdrawn tumors. The vast majority of ESC-methylated genes were downregulated in Dox-withdrawn tumors, whereas a significant portion of kidney-methylated genes remained repressed in these tumors. ESC-methylated genes with decreased expression levels in ESCs and kidney-methylated genes with decreased expression levels in the kidney tissues were examined.
(F) Altered DNA methylation at the DMR of imprinting genes. Note that kidney tumor 2 showed aberrant methylation patterns at *Nnat*, *Impact*, and *Meg3*. In contrast, kidney tumor 1 showed an aberration only at *Nnat*.
See also Figures S4 and S5.

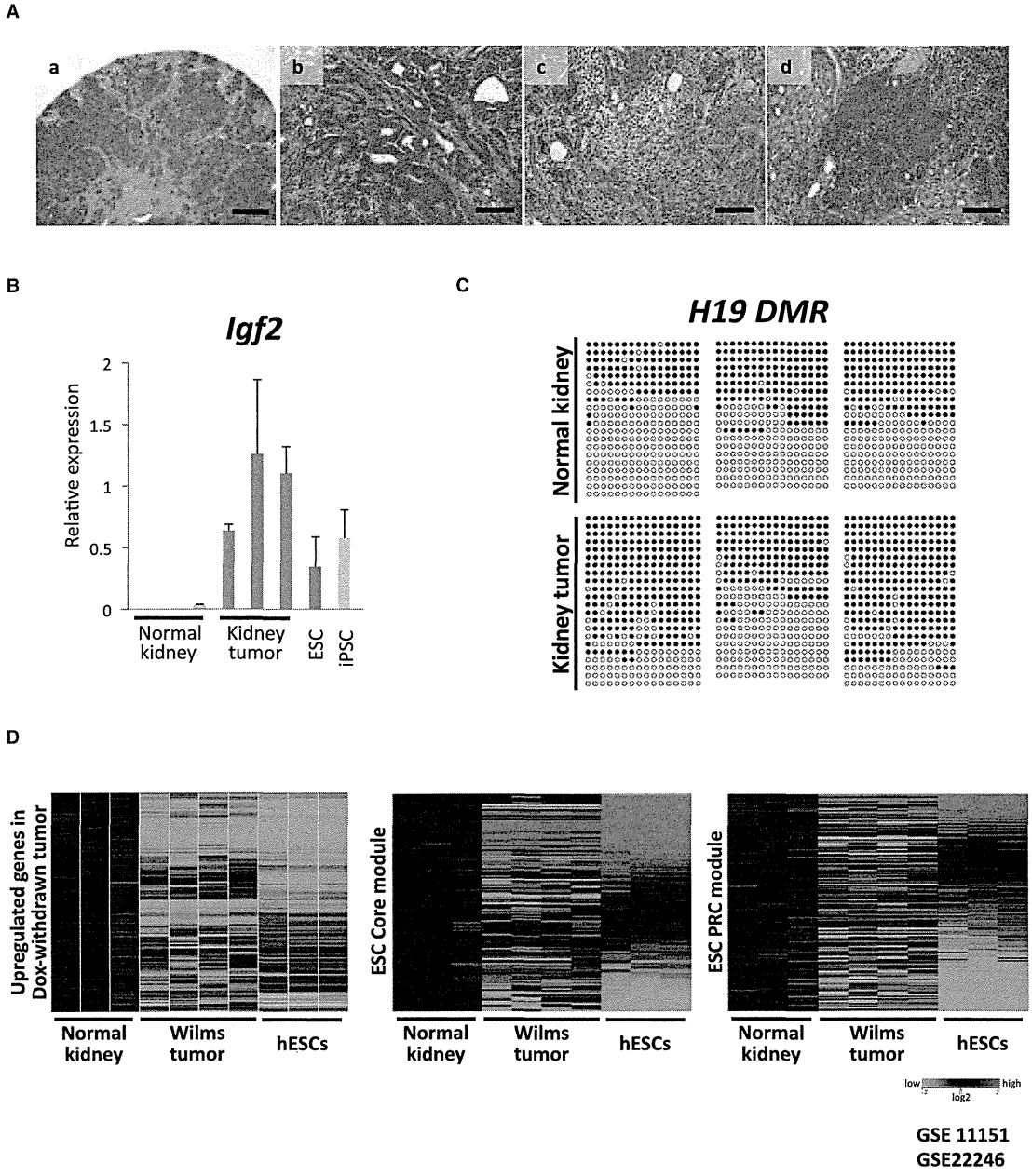

Figure 5. Dox-Withdrawn Kidney Tumors Resemble Wilms Tumors

(A) Representative histological findings of Dox-withdrawn kidney tumors (a–d). Tumors consisted of epithelial (b), stromal (c), and blastema-like (d) compartments, which are histological features of Wilms tumors. Scale bars, 500 μm (a) and 100 μm (b–d).

(B) The results of the qRT-PCR analysis for *Igf2*. *Igf2* was highly expressed in Dox-withdrawn kidney tumors. Data are presented as mean ± SD. The mean level of kidney tumors was set to 1.

(legend continued on next page)

those in normal kidney tissues, hESCs, and RCCs (Figures 5D and S6D) (Aiden et al., 2010). Collectively, kidney tumors induced by the transient expression of reprogramming factors display a number of shared characteristics with Wilms tumor. These findings also indicate that our mouse model may prove useful to uncover the pathogenesis of Wilms tumors.

iPSCs Derived from Dox-Withdrawn Kidney Tumors Contribute to Nonneoplastic Kidney Tissues in Chimeric Mice

We next tried to establish iPSCs from Dox-withdrawn kidney tumor cells. The tumor cell-specific *Lgr5-EGFP* reporter allele defined in this study was utilized to isolate tumor cells (Figures 3D, 3E, and S3E). *Lgr5*-expressing GFP-positive tumor cells were sorted and cultured in vitro with Dox to establish iPSCs from tumor cells (Figure 6A). During the culture of *Lgr5*-expressing tumor cells in vitro, *Nanog* expression at a level comparable to that in pluripotent stem cells was detected as early as 7 days after reprogramming factor induction (Figure 6B), a rate faster than the reprogramming process from normal kidney tubule cells in vitro (Figure S7A). After 2 weeks of culture with Dox exposure, more than 20 alkaline phosphatase (AP)-positive iPSC-like colonies were obtained from 100 *Lgr5*-expressing tumor cells (Figure S7B). We were able to establish Dox-independent iPSC lines from tumor cells at 3 weeks after transgene induction (Figure 6C), suggesting that the Dox-withdrawn tumor cells can be readily reprogrammed into pluripotent stem cells.

Cancers are believed to arise through the accumulation of multiple genetic abnormalities. We next investigated whether genetic abnormalities mandate the emergence of in Dox-withdrawn tumors. Exonic regions of 514 genes that include human-cancer-related genes in transplanted secondary kidney tumors were sequenced using a hybridization selection technique combined with next-generation sequencing (Table S3). Mutations in *Wt1*, *Wtx*, *Ctnnb1*, and *Trp53*, all of which have been identified in a subset of Wilms tumors, were not detected in three tumors examined. In addition, no cancer-related gene mutations were enriched in these tumors (data not shown). Array-based comparative genomic hybridization (CGH) revealed no prevalent chromosomal alteration in tumor samples (Figure S7C).

Finally, we injected the tumor-derived iPSCs into blastocysts to generate chimeric mice. Tumor-derived iPSCs contributed into adult chimeric mice (Figure 6D). Notably, the kidney-tumor-derived iPSCs differentiated into normal-looking kidney tissues (Figures 6E, 6F, and S7D). Moreover, these chimeric mice did not develop tumors even at 24 weeks of age (n = 8). To further demonstrate that tumorigenic cells can be reprogrammed into nonneoplastic cells, we also established iPSCs from the transplanted secondary tumors and confirmed their contribution to nonneoplastic kidney tissues (Figure S7E). These results substantiate that a genetic context of the Dox-withdrawn kidney tumor cells is not determinant of the cancer phenotype and support the conclusion that altered epigenetic regulations cause the abnormal growth in somatic cells, leading to the development of Dox-withdrawn tumors.

DISCUSSION

During somatic cell reprogramming, iPSCs gain the capacity for unlimited growth without particular genetic alterations. Using abbreviated reprogramming factor expression in vivo, we demonstrate that transient expression of reprogramming factors leads to tumor development. Such tumors display altered epigenetic modifications, indicating that epigenetic regulation characteristic of cellular reprogramming may also confer neoplastic growth properties to somatic cells. Intriguingly, Dox-withdrawn tumor cells are readily reprogrammed into pluripotent stem cells by additional 4F expression, indicating that the tumor cells represent a cellular state closer to iPSCs than the original somatic cells. Moreover, kidney tumor cell-derived iPSCs contribute to various somatic cell types and give rise to nonneoplastic kidney cells in mice. These data demonstrate that the abnormal growth of unsuccessfully reprogrammed cells depends predominantly on epigenetic regulations and raise the possibility that particular types of cancer may arise exclusively through altered epigenetic regulation.

Histological features of Dox-withdrawn tumors imply that unsuccessfully reprogrammed cells lack the ability to terminal differentiate along multiple lineages. It is noteworthy that Dox-withdrawn tumor cells fail to repress ESC-PRC targets yet share the activation of ESC core regulatory circuitry and Myc-related genes with pluripotent stem cells. It is conceivable that the repression of ESC-PRC targets would be exclusively associated with the acquisition of pluripotency, whereas activation of ESC core regulatory circuitry and Myc targets lead to self-renewing activity. This notion is also consistent with previous findings that PRC components are important for successful reprogramming in humans (Onder et al., 2012). Notably, the failed repression of the ESC-PRC module was detectable in previously reported partially reprogrammed cells in vitro (Polo et al., 2012), in which the activation of both ESC-Core and ESC-Myc modules had already occurred (Figure S7F). We also found that unsuccessfully reprogrammed kidney cells tend to retain DNA methylation at kidney-specific methylated genes. Considering that global epigenetic reorganization, including changes in both H3K27 methylation and DNA methylation, occurs during the later phase of iPSC generation (Polo et al., 2012), the expected repression of ESC-PRC targets and demethylation of somatic cell-specific genomic methylation might play a role in the final stages of successful somatic cell reprogramming.

Recently, Abad et al. reported that in vivo reprogramming allows the acquisition of totipotent features resulting in embryo-like cyst formation in reprogrammable mice (Abad et al., 2013). However, in the present study, we did not observe such cystic structures in Dox-treated reprogrammable mice.

(C) The bisulfite sequencing analysis revealed increased DNA methylation levels at the *H19* DMR containing two CTCF binding sites in Dox-withdrawn tumors.
(D) The results of the global expression analyses in Wilms tumors. The human orthologs of upregulated genes in Dox-withdrawn tumors and ESC module genes were assessed using previously reported microarray data sets (GSE11151 and GSE22246).
See also Figure S6.

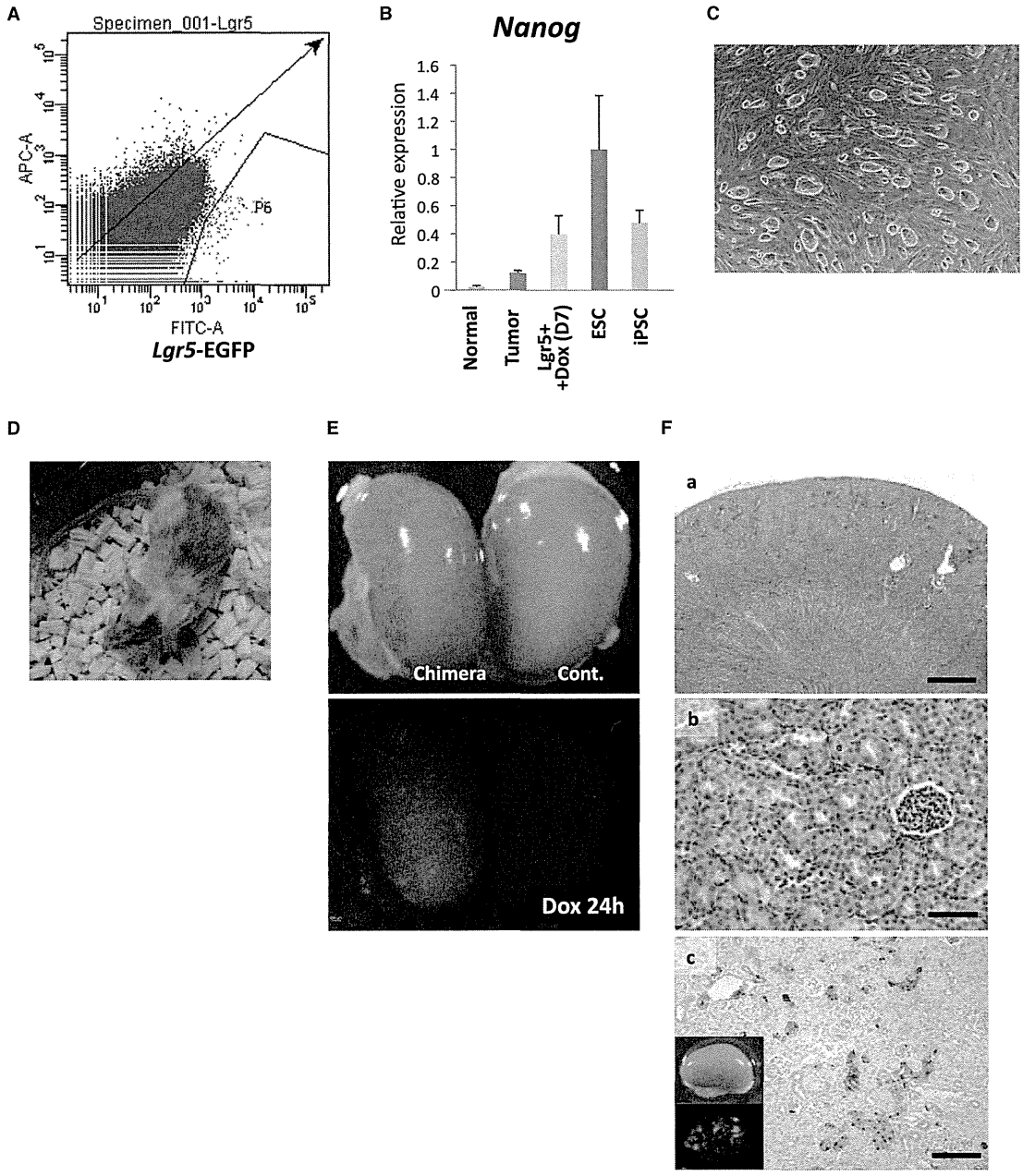

Figure 6. Generation of iPSCs from Dox-Withdrawn Tumors and Their Contribution to Normal-Looking Kidney Tissue

(A) The fluorescence-activated cell sorting analyses of Dox-withdrawn kidney tumor cells in a reprogrammable chimeric mouse with the *Lgr5*-EGFP reporter. GFP-positive *Lgr5*-expressing cells were sorted to exclusively isolate Dox-withdrawn tumor cells.

(B) Dox treatment of *Lgr5*-expressing tumor cells caused the rapid induction of *Nanog*. The *Nanog* levels were examined after seven days of treatment with Dox in vitro. Data are presented as mean ± SD. The level in ESCs was set to 1.

(C) An image of iPSCs derived from *Lgr5*-positive kidney tumor cells.

(legend continued on next page)

Furthermore, teratoma-derived in vivo iPSCs in this study failed to differentiate into placental tissues despite robust fetal contribution upon injection into eight-cell-stage embryos (data not shown), suggesting that not all in vivo iPSCs are totipotent. Because the previous study was conducted using circulating iPSCs recovered in blood, the cell of origin for in vivo reprogramming might affect the acquisition of totipotent features. It should be also noted that Abad et al. utilized germline-transmitted transgenic mice that harbor lentivirus-mediated integration of inducible reprogramming factors (Carey et al., 2009) whereas we examined chimeric mice with transgenes at a targeted locus. The different levels of transgene induction caused by such distinct transgenic systems may underlie differences in the phenotypes observed between these two studies.

Here, we show that failed reprogramming-associated cancers resemble Wilms tumors in terms of histology and molecular characteristics, including aberrant expression of imprinted genes correlated with altered DNA methylation. It is well known that Wilms tumors have characteristics distinct from adult kidney cancers in many aspects. On the basis of our findings in Dox-withdrawn tumors, we discovered that Wilms tumors harbor an activated ESC core regulatory circuitry. This is in sharp contrast to previous findings that most adult cancers do not show activation of ESC core regulatory circuitry (Kim et al., 2010). We also found that many ESC-PRC targets are not repressed in Wilms tumors, despite common repression in many cancers (Ben-Porath et al., 2008; Kim et al., 2010). Gene Ontology analysis revealed that derepressed PRC genes in Wilms tumors include genes involved in kidney development, whereas they are not enriched in derepressed PRC genes in RCCs (data not shown), suggesting that activation of the embryonic kidney transcriptional network is associated with Wilms tumor development. Taken together, strongly active ESC-core regulatory circuitry and derepression of certain ESC-PRC targets may characterize Wilms tumors and may account for the characteristics distinctive of Wilms tumors and adult kidney cancers.

Although we revealed striking similarity between Dox-withdrawn kidney tumors and Wilms tumors, it remains unclear whether reprogramming processes play a role in the development of human Wilms tumors. It has been widely accepted that nephrogenic rests, abnormally persistent clusters of embryonal cells, are the precursors of Wilms tumors. Considering the artificial expression of reprogramming factors in our experimental system, the current study does not provide direct evidence that dedifferentiation is normally involved in the human Wilms tumor development. Yet, based on our findings, it is conceivable that a reprogramming process might cause cell-fate conversion into progenitor-like states, leading to the development of nephrogenic rests required for the early stages of Wilms tumorigenesis. Further detailed analyses using human samples are required to uncover the role of reprogramming in cancer development in humans.

In summary, we demonstrated that premature termination of in vivo reprogramming causes tumor development resembling Wilms tumor. Our findings suggest that altered epigenetic regulations relating to somatic cell reprogramming drive tumorigenesis, highlighting the importance of epigenetic regulation in cancer development.

EXPERIMENTAL PROCEDURES

Generation of OSMK-Inducible ESCs

A 7 kb fragment containing Oct3/4-P2A-Sox2-T2A-Klf4-E2A-c-Myc-ires-mCherry cDNA was generated (Carey et al., 2009) and ligated into the pBS31 vector (Beard et al., 2006). The resulting construct was electroporated into KH2 ESCs to obtain OSKM-inducible ESCs (Beard et al., 2006). OKS-, KMS-, O-, LacZ-inducible ESCs were also generated using the KH2 ESCs system.

Mice

Chimeric mice were generated using reprogramming factor-inducible ESCs by diploid blastocyst injection. *Lgr5-EGFP-ires-CreERT2* mice were obtained from The Jackson Laboratory and were crossed with OSKM-inducible mice to obtain embryos. The compound transgenic MEFs were treated with Dox to establish the OSKM-inducible iPSCs with the *Lgr5-EGFP* reporter allele. All animal experiments were approved by the CiRA Animal Experiment Committee, and the care of the animals was in accordance with institutional guidelines.

Doxycycline Treatment

Mice at 4 or 14 weeks of age were administered 2 mg/ml Dox in their drinking water supplemented with 10 mg/ml sucrose. For cell culture, Dox was used at a concentration of 2 μg/ml.

Secondary Tumor Development

Primary kidney tumors were minced and treated with collagenase (1 U/ml) followed by 0.25% trypsin digestion. The dissociated tumor cells were inoculated subcutaneously into BALB/cSlc-*nu/nu* mice or C.B-17/Icr-*scid*Jcl mice to form transplanted secondary tumors.

RNA Preparation, qRT-PCR and Microarray Analysis

Total RNA was isolated using the RNeasy Plus Mini kit (QIAGEN). The quantitative real-time PCR analysis was performed using the GoTaq qPCR Master Mix (Promega). The specific primer pairs used for amplification are shown in Table S2. The transcript levels were normalized to the *β-actin* level. The microarray analysis was performed using the Mouse Gene 1.0 ST Array (Affymetrix) in accordance with the manufacturer's instructions. All of the data analyses were performed using the GeneSpring GX software program (version 12; Agilent Technology).

DNA Methylation Analyses

The RRBS analysis was performed as described previously (Boyle et al., 2012). The samples were sequenced on an Illumina HiSeq 2000 machine. Three-kilobase regions flanking transcription start site (from −1,500 to +1,500) were analyzed to examine DNA methylation levels. The DNA methylation levels for each gene were determined based on the median of DNA methylation values at CpG sites within the region. The DNA methylation values at CpG sites

(D) Kidney tumor-derived iPSCs can contribute to adult chimeric mice.
(E) No tumor formation was observed in the kidneys of chimeric mice generated with kidney tumor-derived iPSCs. Note that Dox treatment for 24 hr confirmed the contribution of kidney-tumor-derived iPSCs to the normal-looking kidney.
(F) The histological analyses of the kidneys of chimeric mice demonstrated no detectable histological abnormalities (a and b). Kidney-tumor-derived iPSCs labeled with Venus could contribute to normal-looking kidney (c). Scale bars, 500 μm (a) and 100 μm (b, c).
See also Figure S7.

containing higher than 10× coverage in all comparative samples were used for the analysis.

Histological Analysis and Immunostaining

Normal and tumor tissue samples were fixed in 10% buffered formalin for 24 hr and embedded in paraffin. Sections (4 μm) were stained with hematoxylin and eosin (H&E), and serial sections were used for the immunohistochemical analyses. The primary antibodies used were anti-Oct3/4 (1:100 dilution; BD Biosciences), anti-Ki-67 (1:100 dilution; Dako), anti-insulin (1:500 dilution; Dako), anti-BrdU (1:500 dilution; Abcam), anti-2A (1:250 dilution; Millipore), anti-Lin28b (1:100 dilution; Cell Signaling Technology), and anti-GFP (1:500 dilution; Invitrogen).

ACCESSION NUMBERS

The Gene Expression Omnibus accession number for the microarray and RRBS data reported in this paper is GSE52304.

SUPPLEMENTAL INFORMATION

Supplemental Information includes Extended Experimental Procedures, seven figures, and three tables and can be found with this article online at http://dx.doi.org/10.1016/j.cell.2014.01.005.

ACKNOWLEDGMENTS

We are grateful to T. Taya for CGH analysis and S. Sakurai and T. Sato for RRBS analysis. We also thank S. Masui, H. Sakurai, and members in Yamada laboratory for helpful discussions and T. Ukai, K. Osugi, and N. Nishimoto for assistance. The authors were supported in part by a Grant-in-Aid from the Ministry of Education, Culture, Sports, Science, and Technology of Japan (MEXT); the Ministry of Health, Labor, and Welfare of Japan; the JST; the Funding Program for World-Leading Innovative R&D on Science and Technology (FIRST Program) of the Japanese Society for the Promotion of Science (JSPS); the Takeda Science Foundation; and the Naito Foundation. S.Y. is a member without salary of the scientific advisory boards of iPierian, iPS Academia Japan, Megakaryon Corporation, and HEALIOS K. K. Japan. The iCeMS is supported by World Premier International Research Center Initiative, MEXT, Japan.

Received: May 29, 2013
Revised: November 6, 2013
Accepted: January 3, 2014
Published: February 13, 2014

REFERENCES

Abad, M., Mosteiro, L., Pantoja, C., Cañamero, M., Rayon, T., Ors, I., Graña, O., Megías, D., Domínguez, O., Martínez, D., et al. (2013). Reprogramming in vivo produces teratomas and iPS cells with totipotency features. Nature *502*, 340–345.

Aiden, A.P., Rivera, M.N., Rheinbay, E., Ku, M., Coffman, E.J., Truong, T.T., Vargas, S.O., Lander, E.S., Haber, D.A., and Bernstein, B.E. (2010). Wilms tumor chromatin profiles highlight stem cell properties and a renal developmental network. Cell Stem Cell *6*, 591–602.

Barker, N., van Es, J.H., Kuipers, J., Kujala, P., van den Born, M., Cozijnsen, M., Haegebarth, A., Korving, J., Begthel, H., Peters, P.J., and Clevers, H. (2007). Identification of stem cells in small intestine and colon by marker gene Lgr5. Nature *449*, 1003–1007.

Barker, N., Rookmaaker, M.B., Kujala, P., Ng, A., Leushacke, M., Snippert, H., van de Wetering, M., Tan, S., Van Es, J.H., Huch, M., et al. (2012). Lgr5(+ve) stem/progenitor cells contribute to nephron formation during kidney development. Cell Rep. *2*, 540–552.

Beard, C., Hochedlinger, K., Plath, K., Wutz, A., and Jaenisch, R. (2006). Efficient method to generate single-copy transgenic mice by site-specific integration in embryonic stem cells. Genesis *44*, 23–28.

Ben-Porath, I., Thomson, M.W., Carey, V.J., Ge, R., Bell, G.W., Regev, A., and Weinberg, R.A. (2008). An embryonic stem cell-like gene expression signature in poorly differentiated aggressive human tumors. Nat. Genet. *40*, 499–507.

Boyle, P., Clement, K., Gu, H., Smith, Z.D., Ziller, M., Fostel, J.L., Holmes, L., Meldrim, J., Kelley, F., Gnirke, A., and Meissner, A. (2012). Gel-free multiplexed reduced representation bisulfite sequencing for large-scale DNA methylation profiling. Genome Biol. *13*, R92.

Brambrink, T., Foreman, R., Welstead, G.G., Lengner, C.J., Wernig, M., Suh, H., and Jaenisch, R. (2008). Sequential expression of pluripotency markers during direct reprogramming of mouse somatic cells. Cell Stem Cell *2*, 151–159.

Carey, B.W., Markoulaki, S., Hanna, J., Saha, K., Gao, Q., Mitalipova, M., and Jaenisch, R. (2009). Reprogramming of murine and human somatic cells using a single polycistronic vector. Proc. Natl. Acad. Sci. USA *106*, 157–162.

Carey, B.W., Markoulaki, S., Beard, C., Hanna, J., and Jaenisch, R. (2010). Single-gene transgenic mouse strains for reprogramming adult somatic cells. Nat. Methods *7*, 56–59.

Ehrich, M., Nelson, M.R., Stanssens, P., Zabeau, M., Liloglou, T., Xinarianos, G., Cantor, C.R., Field, J.K., and van den Boom, D. (2005). Quantitative high-throughput analysis of DNA methylation patterns by base-specific cleavage and mass spectrometry. Proc. Natl. Acad. Sci. USA *102*, 15785–15790.

Folmes, C.D., Nelson, T.J., Martinez-Fernandez, A., Arrell, D.K., Lindor, J.Z., Dzeja, P.P., Ikeda, Y., Perez-Terzic, C., and Terzic, A. (2011). Somatic oxidative bioenergetics transitions into pluripotency-dependent glycolysis to facilitate nuclear reprogramming. Cell Metab. *14*, 264–271.

Fussner, E., Djuric, U., Strauss, M., Hotta, A., Perez-Iratxeta, C., Lanner, F., Dilworth, F.J., Ellis, J., and Bazett-Jones, D.P. (2011). Constitutive heterochromatin reorganization during somatic cell reprogramming. EMBO J. *30*, 1778–1789.

Hochedlinger, K., Yamada, Y., Beard, C., and Jaenisch, R. (2005). Ectopic expression of Oct-4 blocks progenitor-cell differentiation and causes dysplasia in epithelial tissues. Cell *121*, 465–477.

Hong, H., Takahashi, K., Ichisaka, T., Aoi, T., Kanagawa, O., Nakagawa, M., Okita, K., and Yamanaka, S. (2009). Suppression of induced pluripotent stem cell generation by the p53-p21 pathway. Nature *460*, 1132–1135.

Jones, P.A., and Baylin, S.B. (2002). The fundamental role of epigenetic events in cancer. Nat. Rev. Genet. *3*, 415–428.

Kim, J., Woo, A.J., Chu, J., Snow, J.W., Fujiwara, Y., Kim, C.G., Cantor, A.B., and Orkin, S.H. (2010). A Myc network accounts for similarities between embryonic stem and cancer cell transcription programs. Cell *143*, 313–324.

Kobayashi, A., Valerius, M.T., Mugford, J.W., Carroll, T.J., Self, M., Oliver, G., and McMahon, A.P. (2008). Six2 defines and regulates a multipotent self-renewing nephron progenitor population throughout mammalian kidney development. Cell Stem Cell *3*, 169–181.

Maherali, N., Sridharan, R., Xie, W., Utikal, J., Eminli, S., Arnold, K., Stadtfeld, M., Yachechko, R., Tchieu, J., Jaenisch, R., et al. (2007). Directly reprogrammed fibroblasts show global epigenetic remodeling and widespread tissue contribution. Cell Stem Cell *1*, 55–70.

Meissner, A., Gnirke, A., Bell, G.W., Ramsahoye, B., Lander, E.S., and Jaenisch, R. (2005). Reduced representation bisulfite sequencing for comparative high-resolution DNA methylation analysis. Nucleic Acids Res. *33*, 5868–5877.

Mikkelsen, T.S., Ku, M., Jaffe, D.B., Issac, B., Lieberman, E., Giannoukos, G., Alvarez, P., Brockman, W., Kim, T.K., Koche, R.P., et al. (2007). Genome-wide maps of chromatin state in pluripotent and lineage-committed cells. Nature *448*, 553–560.

Mikkelsen, T.S., Hanna, J., Zhang, X., Ku, M., Wernig, M., Schorderet, P., Bernstein, B.E., Jaenisch, R., Lander, E.S., and Meissner, A. (2008). Dissecting direct reprogramming through integrative genomic analysis. Nature *454*, 49–55.

Ogawa, O., Eccles, M.R., Szeto, J., McNoe, L.A., Yun, K., Maw, M.A., Smith, P.J., and Reeve, A.E. (1993). Relaxation of insulin-like growth factor II gene imprinting implicated in Wilms' tumour. Nature *362*, 749–751.

Ohta, S., Nishida, E., Yamanaka, S., and Yamamoto, T. (2013). Global splicing pattern reversion during somatic cell reprogramming. Cell Rep. *5*, 357–366.

Okita, K., Ichisaka, T., and Yamanaka, S. (2007). Generation of germline-competent induced pluripotent stem cells. Nature *448*, 313–317.

Onder, T.T., Kara, N., Cherry, A., Sinha, A.U., Zhu, N., Bernt, K.M., Cahan, P., Marcarci, B.O., Unternaehrer, J., Gupta, P.B., et al. (2012). Chromatin-modifying enzymes as modulators of reprogramming. Nature *483*, 598–602.

Polo, J.M., Anderssen, E., Walsh, R.M., Schwarz, B.A., Nefzger, C.M., Lim, S.M., Borkent, M., Apostolou, E., Alaei, S., Cloutier, J., et al. (2012). A molecular roadmap of reprogramming somatic cells into iPS cells. Cell *151*, 1617–1632.

Rais, Y., Zviran, A., Geula, S., Gafni, O., Chomsky, E., Viukov, S., Mansour, A.A., Caspi, I., Krupalnik, V., Zerbib, M., et al. (2013). Deterministic direct reprogramming of somatic cells to pluripotency. Nature *502*, 65–70.

Samavarchi-Tehrani, P., Golipour, A., David, L., Sung, H.K., Beyer, T.A., Datti, A., Woltjen, K., Nagy, A., and Wrana, J.L. (2010). Functional genomics reveals a BMP-driven mesenchymal-to-epithelial transition in the initiation of somatic cell reprogramming. Cell Stem Cell *7*, 64–77.

Sridharan, R., Tchieu, J., Mason, M.J., Yachechko, R., Kuoy, E., Horvath, S., Zhou, Q., and Plath, K. (2009). Role of the murine reprogramming factors in the induction of pluripotency. Cell *136*, 364–377.

Stadtfeld, M., Apostolou, E., Akutsu, H., Fukuda, A., Follett, P., Natesan, S., Kono, T., Shioda, T., and Hochedlinger, K. (2010a). Aberrant silencing of imprinted genes on chromosome 12qF1 in mouse induced pluripotent stem cells. Nature *465*, 175–181.

Stadtfeld, M., Maherali, N., Borkent, M., and Hochedlinger, K. (2010b). A reprogrammable mouse strain from gene-targeted embryonic stem cells. Nat. Methods *7*, 53–55.

Steenman, M.J., Rainier, S., Dobry, C.J., Grundy, P., Horon, I.L., and Feinberg, A.P. (1994). Loss of imprinting of IGF2 is linked to reduced expression and abnormal methylation of H19 in Wilms' tumour. Nat. Genet. *7*, 433–439.

Takahashi, K., and Yamanaka, S. (2006). Induction of pluripotent stem cells from mouse embryonic and adult fibroblast cultures by defined factors. Cell *126*, 663–676.

Takahashi, K., Tanabe, K., Ohnuki, M., Narita, M., Ichisaka, T., Tomoda, K., and Yamanaka, S. (2007). Induction of pluripotent stem cells from adult human fibroblasts by defined factors. Cell *131*, 861–872.

Tchieu, J., Kuoy, E., Chin, M.H., Trinh, H., Patterson, M., Sherman, S.P., Aimiuwu, O., Lindgren, A., Hakimian, S., Zack, J.A., et al. (2010). Female human iPSCs retain an inactive X chromosome. Cell Stem Cell *7*, 329–342.

Wernig, M., Meissner, A., Foreman, R., Brambrink, T., Ku, M., Hochedlinger, K., Bernstein, B.E., and Jaenisch, R. (2007). In vitro reprogramming of fibroblasts into a pluripotent ES-cell-like state. Nature *448*, 318–324.

Woltjen, K., Michael, I.P., Mohseni, P., Desai, R., Mileikovsky, M., Hämäläinen, R., Cowling, R., Wang, W., Liu, P., Gertsenstein, M., et al. (2009). piggyBac transposition reprograms fibroblasts to induced pluripotent stem cells. Nature *458*, 766–770.

Yamada, Y., Jackson-Grusby, L., Linhart, H., Meissner, A., Eden, A., Lin, H., and Jaenisch, R. (2005). Opposing effects of DNA hypomethylation on intestinal and liver carcinogenesis. Proc. Natl. Acad. Sci. USA *102*, 13580–13585.

Yusenko, M.V., Kuiper, R.P., Boethe, T., Ljungberg, B., van Kessel, A.G., and Kovacs, G. (2009). High-resolution DNA copy number and gene expression analyses distinguish chromophobe renal cell carcinomas and renal oncocytomas. BMC Cancer *9*, 152.

Cancer Letters 342 (2014) 60–69

Contents lists available at ScienceDirect

Cancer Letters

journal homepage: www.elsevier.com/locate/canlet

Non-alcoholic steatohepatitis and preneoplastic lesions develop in the liver of obese and hypertensive rats: Suppressing effects of EGCG on the development of liver lesions

Takahiro Kochi [a], Masahito Shimizu [a,*], Daishi Terakura [a], Atsushi Baba [a], Tomohiko Ohno [a], Masaya Kubota [a], Yohei Shirakami [a], Hisashi Tsurumi [a], Takuji Tanaka [b], Hisataka Moriwaki [a]

[a] Department of Medicine, Gifu University Graduate School of Medicine, Gifu, Japan
[b] Department of Tumor Pathology, Gifu University Graduate School of Medicine, Gifu, Japan

ARTICLE INFO

Article history:
Received 16 May 2013
Received in revised form 8 August 2013
Accepted 19 August 2013

Keywords:
Obesity
Hypertension
Liver fibrosis
Liver tumorigenesis
EGCG

ABSTRACT

Non-alcoholic steatohepatitis (NASH), which involves hepatic inflammation and fibrosis, is associated with liver carcinogenesis. The activation of the renin-angiotensin system (RAS), which plays a key role in blood pressure regulation, promotes hepatic fibrogenesis. In this study, we investigated the effects of (−)-epigallocatechin-3-gallate (EGCG), a major component of green tea catechins, on the development of glutathione *S*-transferase placental form (GST-P)-positive (GST-P$^+$) foci, a hepatic preneoplastic lesion, in SHRSP.Z-*Lepr*^{fa}/IzmDmcr (SHRSP-ZF) obese and hypertensive rats. Male 7-week-old SHRSP-ZF rats and control non-obese and normotensive WKY rats were fed a high fat diet and received intraperitoneal injections of carbon tetrachloride twice a week for 8 weeks. The rats were also provided tap water containing 0.1% EGCG during the experiment. SHRSP-ZF rats presented with obesity, insulin resistance, dyslipidemia, an imbalance of adipokines in the serum, and hepatic steatosis. The development of GST-P$^+$ foci and liver fibrosis was markedly accelerated in SHRSP-ZF rats compared to that in control rats. Additionally, in SHRSP-ZF rats, RAS was activated and inflammation and oxidative stress were induced. Administration of EGCG, however, inhibited the development of hepatic premalignant lesions by improving liver fibrosis, inhibiting RAS activation, and attenuating inflammation and oxidative stress in SHRSP-ZF rats. In conclusion, obese and hypertensive SHRSP-ZF rats treated with a high fat diet and carbon tetrachloride displayed the histopathological and pathophysiological characteristics of NASH and developed GST-P$^+$ foci hepatic premalignant lesions, suggesting the model might be useful for the evaluation of NASH-related liver tumorigenesis. EGCG might also be able to prevent NASH-related liver fibrosis and tumorigenesis.

1. Introduction

Non-alcoholic fatty liver disease (NAFLD), which is strongly associated with obesity, diabetes mellitus, and the metabolic syndrome, is becoming one of the most common liver diseases worldwide. NAFLD ranges from simple steatosis to non-alcoholic steatohepatitis (NASH), which is a severe condition of inflamed fatty liver that can progress to hepatic fibrosis, cirrhosis, or even hepatocellular carcinoma (HCC) [1,2]. HCC often occurs in patients with NASH, especially in those with advanced fibrosis and cirrhosis, and the occurrence of HCC is the strongest predictor of mortality in patients with advanced fibrosis [3]. Therefore, in order to improve the prognosis of the patients with NASH, it is necessary to elucidate the pathological mechanisms implicated in the progression of liver fibrosis and HCC development. Several pathophysiological mechanisms explaining the development of HCC in NASH have been described, including the emergence of insulin resistance, induction of chronic inflammation and oxidative stress, and an imbalance of adipokines [1–6]. However, appropriate animal models to evaluate NASH-related liver fibrosis and carcinogenesis have not yet been generated.

Recently, angiotensin-II (AT-II) has been implicated as an important molecule in the progression of liver fibrosis and steatosis [7–9]. AT-II is a component of the renin-angiotensin system (RAS), a key regulator of arterial pressure, and has been shown to induce the contractility and proliferation of hepatic stellate cells (HSCs), which play a pivotal role in liver fibrogenesis [7–9]. RAS is frequently activated in patients with hepatic cirrhosis [8]. Activation of RAS has also been implicated in the etiology of hypertension, obesity, and metabolic syndrome [10]. These findings are significant when considering NASH-related liver carcinogenesis because most patients with NASH that develop HCC experience complications with obesity, diabetes, hypertension, and cirrhosis

* Corresponding author. Address: Department of Gastroenterology, Gifu University Graduate School of Medicine, 1-1 Yanagido, Gifu 501-1194, Japan. Tel.: +81 58 230 6313; fax: +81 58 230 6310.
E-mail address: shimim-gif@umin.ac.jp (M. Shimizu).

0304-3835/$ - see front matter © 2013 Elsevier Ireland Ltd. All rights reserved.
http://dx.doi.org/10.1016/j.canlet.2013.08.031

[11]. In addition, AT-II might play a role in the induction of oxidative stress and chronic inflammation in the liver [12,13], both of which are critically involved in the pathogenesis and progression of NASH and the related development of HCC [1–5]. These reports indicate that targeting RAS activation, which is associated with obesity and hypertension, might be an effective strategy to inhibit NASH-related liver carcinogenesis.

The SHRSP.Z-*Lepr*^{fa}/IzmDmcr (SHRSP-ZF) rat is an obese and hypertensive rat, established by crossing stroke-prone spontaneously hypertensive rats (SHRSP) with Zucker Fatty (ZF) rats [14]. SHRSP-ZF rats inherit the leptin receptor *OB-ob* gene mutation found in ZF rats and become obese while developing hypertension. Therefore, the phenotype resembles that of human metabolic syndrome. The rats may thus be a useful tool for investigating the molecular mechanisms underlying metabolic syndrome [15,16]. We therefore considered that appropriate treatment(s) to the SHRSP-ZF rats enable us to establish a novel animal model of NASH and NASH-related hepatocarcinogenesis that mimics those of humans and to use as a preclinical animal model for chemoprevention studies for the diseases.

In the present study, we aimed to create a new NASH-related liver tumorigenesis rat model that appropriately reflects the pathological conditions of human NASH by using SHRSP-ZF rats. We also investigated the potential preventive effects of (−)-epigallocatechin-3-gallate (EGCG), a green tea catechin (GTC), on liver fibrosis, steatosis, and tumorigenesis using this rodent model because green tea is considered to prevent metabolic disorders, including obesity, insulin resistance, hypertension, and NAFLD [17–19], as well as possesses anticancer and cancer chemopreventive properties in various organs, including the liver [20–23]. Glutathione *S*-transferase placental form (GST-P)-positive (GST-P$^+$) foci are frequently used as an indicator of preneoplastic lesions for HCC of rats, since this biomarker shows good correlations with long term carcinogenicity results [24]. We evaluated liver tumorigenesis and chemopreventive efficacy of EGCG in the SHRSP-ZF rats using GST-P$^+$ foci as a biomarker.

2. Materials and methods

2.1. Animals and chemicals

Six-week-old male SHRSP-ZF rats and control Wister Kyoto (WKY) rats, which are normotensive and do not present with obesity, were obtained from Japan SLC (Shizuoka, Japan) and humanely maintained at Gifu University Life Science Research Center in accordance with the Institutional Animal Care Guidelines. High-fat diet 32 (HFD, 507.6 kcal/100 g) with 56.7% fat derived calories was purchased from CLEA Japan (Tokyo, Japan). Carbon tetrachloride (CCl_4) was purchased from Sigma (St. Louis, MO, USA). EGCG was obtained from Mitsui Norin (Tokyo, Japan).

2.2. Experimental procedure

In a preliminary study, we confirmed that the development of preneoplastic lesions, GST-P$^+$ foci, was observed in the liver of WKY and SHRSP-ZF rats only when they were treated with both HFD and CCl_4 (data not shown). Therefore, all rats were fed a pelleted HFD throughout the experiment and received CCl_4 in the present study. After 1 week of acclimatization, 20 WKY rats (Groups 1 and 2; 10 rats for each group) and 20 SHRSP-ZF rats (Groups 3 and 4; 10 rats for each group) were randomly divided into 2 groups. All rats received an intraperitoneal injection of CCl_4 (0.5 mL/kg body weight) twice a week for 8 weeks. At the start of the intraperitoneal injections, the rats in Groups 2 and 4 were provided tap water containing 0.1% EGCG, while the rats in Groups 1 and 3 were provided tap water throughout the experiment. The concentration of EGCG (0.1%), which was established according to the findings of previous chemopreventive studies [22,23] was within the physiological range observed in humans after daily intake of GTCs on a per unit body weight basis [25]. At the end of the experiment (15 weeks of age), all rats were killed by CO_2 asphyxiation, and the development of hepatic steatosis, fibrosis, and GST-P$^+$ foci was determined.

2.3. Histopathological and immunohistochemical examinations

Maximum sagittal sections of 3 sublobes were used for histopathological examination. For all experimental groups, 4 μm-thick sections of formalin-fixed and paraffin-embedded livers were stained with hematoxylin & eosin (H&E) for conventional histopathology or with Azan stain to observe liver fibrosis [26]. The histological features of the livers were evaluated using the NAFLD activity score (NAS) system [27]. The immunohistochemistry of α-smooth muscle actin (α-SMA) [26] and GST-P [28] was performed using primary anti-α-SMA (DAKO, Glostrup, Denmark) and anti-GST-P (MBL, Nagoya, Japan) antibodies, respectively, by using paraffin-embedded sections. In order to evaluate the oxidative stress and lipid peroxidation in the liver, immunohistochemical staining for 8-hydroxy-2′-deoxyguanosine (8-OHdG, NIKKEN SEIL, Shizuoka, Japan) and 4-hydroxy-2′-nonenal (4-HNE, NIKKEN SEIL) of paraffin-embedded sections was performed. Immunohistochemical staining for Mac-1 (Abcam, Cambridge, MA, USA) was also performed on the paraffin-embedded sections to evaluate the infiltration of macrophages in the liver. The Azan- and α-SMA-positive areas were quantified using BZ-Analyzer-II software (KEYENCE, Osaka, Japan) [29]. GST-P$^+$ foci, which consisted of 3 or more positive cells, were counted as hepatic preneoplastic lesions, as previously described [30], and its multiplicity was assessed on a unit area basis (per cm^2). The assessment for GST-P$^+$ foci development and the NAS scoring system were blinded from each other.

2.4. RNA extraction and quantitative real-time reverse transcription-polymerase chain reaction analysis

Total RNA was isolated from the livers of experimental rats using the RNAqueous-4PCR kit (Ambion Applied Biosystems, Austin, TX, USA). cDNA was amplified from 0.2 μg of total RNA using the SuperScript III First-Strand Synthesis System (Invitrogen, Carlsbad, CA, USA). Quantitative real-time reverse transcription-PCR (RT-PCR) analysis was performed using specific primers that amplify *tumor necrosis factor (TNF)-α, interleukin (IL)-1β, IL-6, monocyte chemoattractant protein-1 (MCP-1), plasminogen activator inhibitor-1 (PAI-1), transforming growth factor (TGF)-β1, α-SMA, procollagen-1, tissue inhibitor of metalloproteinases (TIMP)-1, TIMP-2, matrix metalloproteinases (MMP)-2, MMP-9, angiotensin-converting enzyme (ACE), AT-II type 1 receptor (AT-1R), glutathione peroxidase (GPx), catalase (CAT),* and *glyceraldehyde-3-phosphate dehydrogenase (GAPDH)* genes. The sequences of *TNF-α, IL-1β, IL-6, MCP-1, PAI-1, TIMP-1, TIMP-2, MMP-2, MMP-9, ACE,* and *AT-1R* primers, which were obtained from Primer-BLAST (http://www.ncbi.nlm.nih.gov/tools/primer-blast/), are shown in Supplemental Table S1. The sequences of other primers are described in a previous report [31]. Each sample was analyzed on a LightCycler Nano (Roche Diagnostics, GmbH, Mannheim, Germany) with FastStart Essential DNA Green Master (Roche Diagnostics). Parallel amplification of *GAPDH* was used as the internal control.

2.5. Protein extraction and western blot analysis

Total protein was extracted from the livers of experimental rats and equivalent amounts of proteins (20 μg/lane) were examined by western blot analysis [23]. The primary antibody for cytochrome P450 2E1 (CYP2E1) was purchased from Abcam. Primary antibodies for c-Jun NH2-terminal kinase (JNK), phosphorylated JNK (p-JNK), and GAPDH were obtained from Cell Signaling Technology (Beverly, MA, USA). The antibody to GAPDH served as the loading control.

2.6. Clinical chemistry

The blood samples collected from the inferior vena cava of the rats at the time of killing after 6 h of fasting were used for chemical analyses. The serum levels of TNF-α (R&D Systems, Minneapolis, MN, USA), IL-6 (R&D Systems), insulin (Shibayagi, Gunma, Japan), glucose (BioVision Research Products, Mountain View, CA, USA), adiponectin (Shibayagi), leptin (Shibayagi), total cholesterol (Wako Pure Chemical, Osaka, Japan), triglyceride (Wako Pure Chemical), non-esterified fatty acid (NEFA) (Wako Pure Chemical), and AT-II (USCN Life Science Inc, Wuhan, China) were determined by enzyme immunoassay according to the manufacturers' protocols. The serum levels of aspartate aminotransferase (AST) and alanine aminotransferase (ALT) were measured using a standard clinical automatic analyzer (type 7180; Hitachi, Tokyo, Japan).

2.7. Hepatic hydroxyproline analysis

The hepatic hydroxyproline content (μmol/g wet liver) was quantified colorimetrically in duplicate samples from approximately 200 mg wet-weight of liver tissues [32].

2.8. Oxidative stress analysis

Serum hydroperoxide levels, one of the markers for oxidative stress, were determined using the derivatives of reactive oxygen metabolites (d-ROM) test (FREE Carpe Diem; Diacron s.r.l., Grosseto, Italy). After equalizing the protein contents, hepatic levels of malondialdehyde (MDA) were evaluated using an MDA assay kit (Northwest Life Science Specialties, Vancouver, WA, USA).

Table 1
Body, liver, and adipose tissue weights and BMI of the experimental rats.

Group no.	Strain	EGCG	No. of rats	Body weight (g)	Relative organ weight (g/100 g body weight)		BMI[b]
					Liver	Adipose[a]	
G1	WKY	–	10	312.5 ± 13.3[c]	4.1 ± 1.0	1.9 ± 0.4	6.0 ± 0.4
G2	WKY	+	10	296.8 ± 19.4	3.7 ± 0.2	2.0 ± 0.2	6.0 ± 0.3
G3	SHRSP-ZF	–	10	352.9 ± 37.9[d]	5.6 ± 0.6[d]	2.8 ± 0.2[d]	8.3 ± 0.9[d]
G4	SHRSP-ZF	+	10	421.1 ± 38.7[e,f]	6.4 ± 0.4[e]	2.8 ± 0.1[e]	9.4 ± 0.7[e,f]

[a] White adipose tissue of the periorchis and retroperitoneum.
[b] Body mass index.
[c] Mean ± SD.
[d] Significantly different from group 1 by Tukey–Kramer multiple comparison test ($P < 0.05$).
[e] Significantly different from group 2 by Tukey–Kramer multiple comparison test ($P < 0.05$).
[f] Significantly different from group 3 by Tukey–Kramer multiple comparison test ($P < 0.01$).

2.9. Statistical analysis

All data are presented as mean ± SD and were analyzed using the GraphPad In-Stat software program version 3.05 (GraphPad Software, San Diego, CA) for Macintosh. One-way analysis of variance (ANOVA) was used to make comparison between the groups. If the ANOVA analysis indicated significant differences, the Tukey–Kramer multiple comparisons test was performed to compare the mean values among the groups. The differences were considered significant when the two-sided P value was less than 0.05.

3. Results

3.1. General observations

The body weights, relative weights of liver and adipose tissues, and body mass index (BMI) of the SHRSP-ZF rats were significantly higher than those of the WKY rats, regardless of EGCG treatment (Table 1; $P < 0.05$). In SHRSP-ZF rats, the body weights and BMI of the EGCG-treated rats were significantly higher than those of untreated rats ($P < 0.01$), suggesting that EGCG might prevent body weight loss caused by liver fibrosis. During the experiment, EGCG in the drinking water did not cause any clinical symptoms for toxicity. Histopathological examinations also revealed the absence of toxicity from EGCG in the liver, kidney, and spleen (data not shown).

3.2. Effects of EGCG on the development of hepatic preneoplastic lesions and histopathology in the experimental rats

Irrespective of the rat strain, GST-P$^+$ foci were observed in the livers of rats from all groups at the termination of the experiment (Fig. 1A). However, the number of foci was significantly increased, by approximately 5.2-fold, in SHRSP-ZF rats compared to that in WKY rats (Fig. 1B; $P < 0.001$), indicating that obesity and hypertension play a critical role in accelerating the development of hepatic preneoplastic lesions. On the other hand, EGCG treatment significantly inhibited the development of GST-P$^+$ foci in obese and hypertensive SHRSP-ZF rats ($P < 0.001$).

Steatosis with ballooning and/or Mallory-Deng body (Fig. 1C and D), and the infiltration of macrophages (Fig. 1E), which are a recognized feature of alcoholic hepatitis and NASH [27], were observed in the liver of both strains of rats that received CCl_4. However, the NAS scores, which reflect the sum of steatosis, hepatocyte ballooning, and lobular inflammation [27], were significantly higher in the SHRSP-ZF rats than in the WKY rats (Fig. 1F; $P < 0.01$). When given EGCG, the NAS score was improved in SHRSP-ZF rats ($P < 0.01$).

3.3. Effects of EGCG on liver fibrosis in the experimental rats

Azan-stained sections indicated that SHRSP-ZF and WKY rats developed liver fibrosis after CCl_4 injection. However, the degree of fibrosis was more severe in SHRSP-ZF rats; densitometric analysis showed that the hepatic fibrosis area in SHRSP-ZF rats was significantly larger than that in WKY rats (Fig. 2A; $P < 0.001$). Densitometric analysis of α-SMA immunohistochemistry also showed that the α-SMA-immunoreactive areas, which reflect the activation of HSCs, were remarkably increased in the livers of SHRSP-ZF rats in comparison with those in the livers of WKY rats (Fig. 2B; $P < 0.001$). However, administration of EGCG through drinking water significantly improved CCl_4-induced liver fibrosis and inhibited the activation of HSCs in SHRSP-ZF rats (Fig. 2A and B; $P < 0.001$).

Similar findings were observed in the measurements of the hepatic hydroxyproline contents. The amount of hydroxyproline in the liver, which was approximately 7.2-fold higher in SHRSP-ZF rats than in WKY rats ($P < 0.001$), decreased significantly after EGCG treatment (Fig. 2C; $P < 0.01$). Moreover, quantitative real-time RT-PCR analysis revealed that, in the livers of SHRSP-ZF rats, EGCG significantly decreased the expression levels of *MMP-2*, *MMP-9*, *TIMP-1*, *TIMP-2*, *α-SMA*, *procollagen-1*, *TGF-β1*, and *PAI-1* mRNA ($P < 0.05$), all of which were remarkably higher in SHRSP-ZF rats than in WKY rats (Fig. 2D; $P < 0.05$).

3.4. Effects of EGCG on serum levels of AT-II and hepatic expression of ACE and AT-1R mRNA in the experimental rats

Hyperactivity of RAS is closely associated with liver fibrosis and carcinogenesis [8,33]. Therefore, the serum levels of AT-II and the expression levels of RAS components, including *ACE* and *AT-1R* mRNA in the liver, were investigated. The serum level of AT-II was markedly elevated in SHRSP-ZF rats compared to that in WKY rats ($P < 0.001$), but was significantly decreased by EGCG treatment (Fig. 3A; $P < 0.05$). In SHRSP-ZF rats, there was a marked increase in the expression levels of *ACE* and *AT-1R* mRNA in the liver ($P < 0.05$); however, EGCG significantly decreased the expression levels of these mRNA (Fig. 3B; $P < 0.05$).

3.5. Effects of EGCG on oxidative stress, lipid peroxidation in the liver, and hepatic expression of CYP2E1, JNK, and p-JNK proteins in the experimental rats

Hepatic oxidative stress and lipid peroxidation are implicated in the hepatic fibrogenesis, progression of fatty livers to NASH, and development of HCC [4,6]. Therefore, the levels of oxidative stress and antioxidant biomarkers in the experimental rats were next assessed. SHRSP-ZF rats showed a significant increase in serum

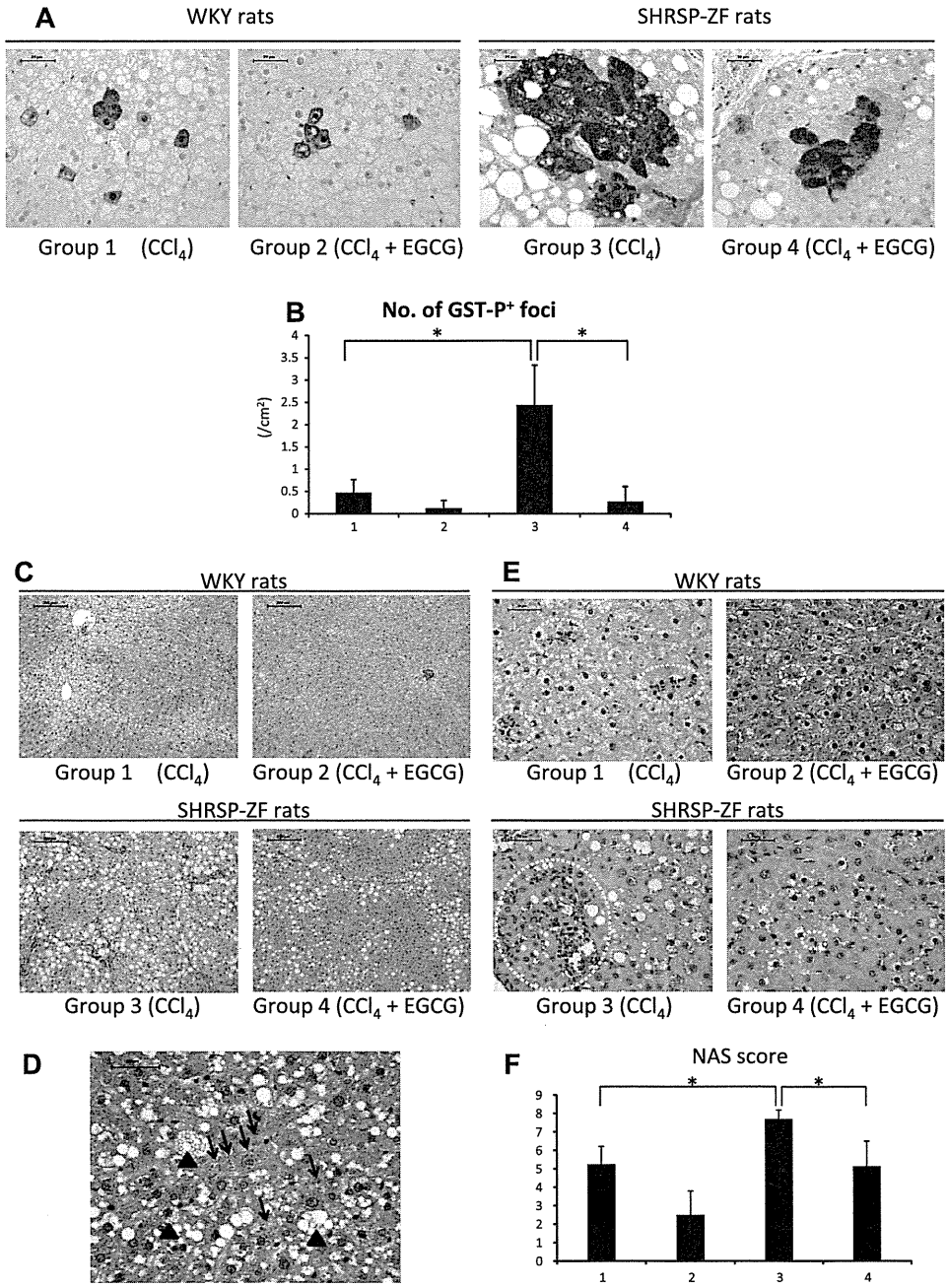

Fig. 1. Effects of EGCG on the development of GST-P$^+$ foci and histopathology in the livers of the experimental rats. (A) Representative photomicrographs of GST-P$^+$ foci and (B) the average number of GST-P$^+$ foci that developed in the livers of the experimental rats. Group 1: WKY rats treated without EGCG, Group 2: WKY rats treated with EGCG, Group 3: SHRSP-ZF rats treated without EGCG, and Group 4: SHRSP-ZF rats treated with EGCG. (C and D) Histopathology of the livers of the experimental rats. H&E staining of liver paraffin sections show steatosis with fibrosis and fatty degeneration in the WKY and SHRSP-ZF rats that were fed HFD and received CCl_4. (D) High magnification of view shows liver cell ballooning (arrow heads) and Mallory-Deng body (arrows) in the liver of a SHRSP-ZF rat from Group 3. (E) The results of the immunohistochemical analysis of Mac-1 in the livers of the experimental rats. Infiltration of macrophages is indicated with circular broken lines. (F) The NAS score (steatosis, inflammation, and ballooning) was determined based on the histopathological analysis. Bars are (A and C) 200 μm and (D and E) 50 μm. The values are expressed as mean ± SD. $^*P < 0.001$.

d-ROM levels, which reflect serum hydroperoxide levels ($P < 0.001$), but this increase was significantly attenuated by EGCG treatment (Fig. 4A; $P < 0.05$). The increased levels of hepatic MDA, a marker of hepatic lipid peroxidation, in SHRSP-ZF rats ($P < 0.05$) were also reduced by EGCG treatment (Fig. 4B; $P < 0.05$). These findings are consistent with the results of immunohistochemical analysis for 8-OHdG, a product of hydroxyl radical-induced oxidative damage in DNA, and 4-HNE, a marker of lipid peroxidation.

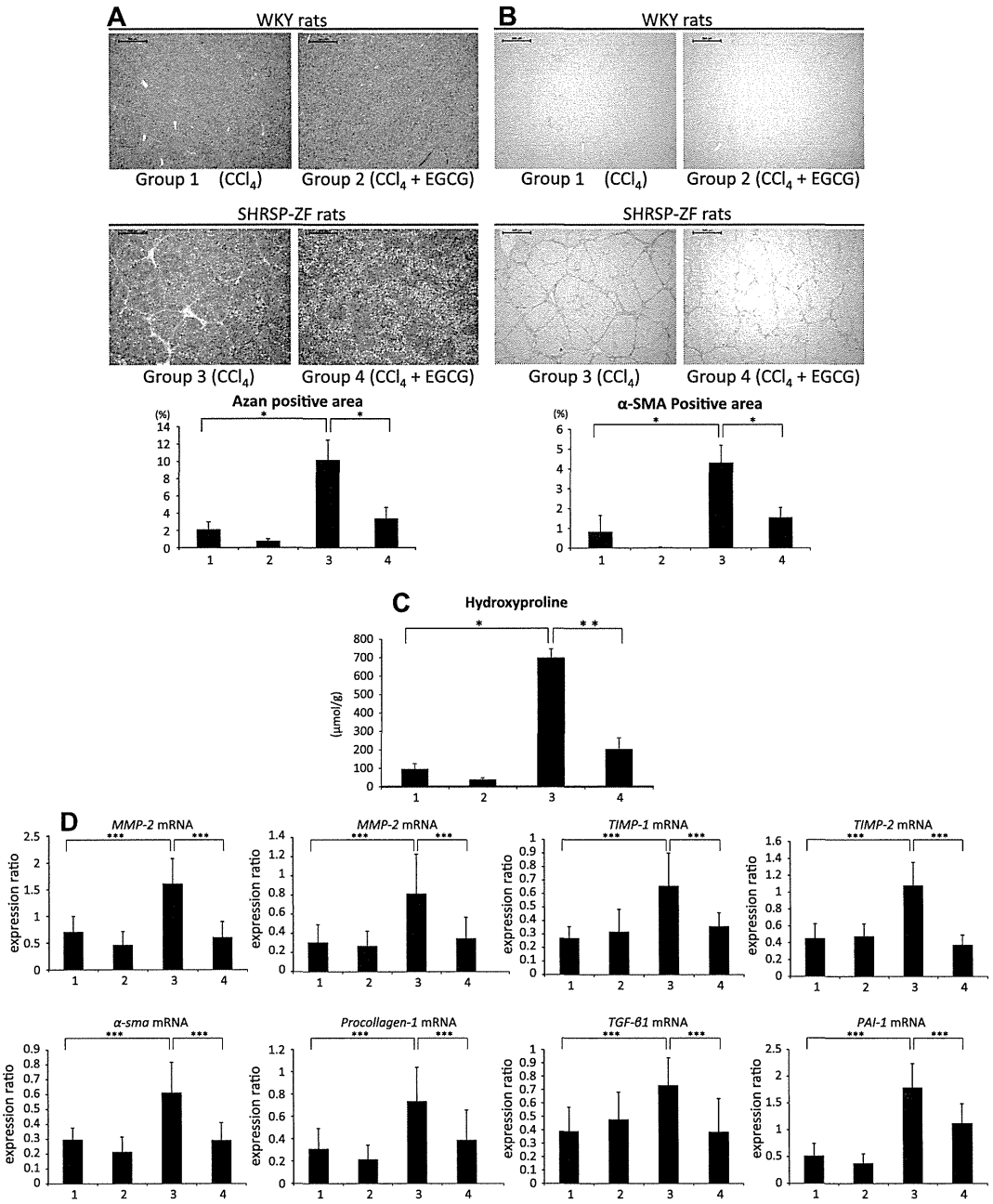

Fig. 2. Effects of EGCG on hepatic fibrosis in the experimental rats. (A) Representative photomicrographs of liver sections stained with Azan stain to show fibrosis (upper panels). The hepatic fibrosis area was evaluated by Azan stain (lower panel). (B) Immunohistochemical detection of α-SMA expression in the livers of the experimental rats (upper panels). The α-SMA-positive area, which shows the activation of HSCs, was evaluated using an image analyzer (lower panel). (C) The hepatic hydroxyproline content was quantified colorimetrically. (D) Total RNA was isolated from the livers of experimental rats, and the expression levels of MMP-2, MMP-9, TIMP-1, TIMP-2, α-SMA, TGF-β1, procollagen-1, and PAI-1 mRNA were examined by quantitative real-time RT-PCR by using specific primers. Bars are 200 μm. The values are expressed as mean ± SD. $^{*}P < 0.001$, $^{**}P < 0.01$, $^{***}P < 0.05$.

The expression levels of 8-OHdG and 4-HNE proteins were markedly increased in the hepatocytes of SHRSP-ZF rats, but they were decreased by EGCG treatment (Fig. 4C). Furthermore, the increased levels of hepatic CYP2E1 and p-JNK proteins, both of which are critically important in HFD-induced NASH development by promoting oxidative stress and inflammation [34,35] in SHRSP-ZF rats were also decreased by EGCG treatment (Fig. 4D). On the other hand, the reduced expression levels of *GPx* and *CAT* mRNA, which encode antioxidant enzymes, in SHRSP-ZF rats ($P < 0.05$) were effectively restored by EGCG treatment (Fig. 4E; $P < 0.05$).

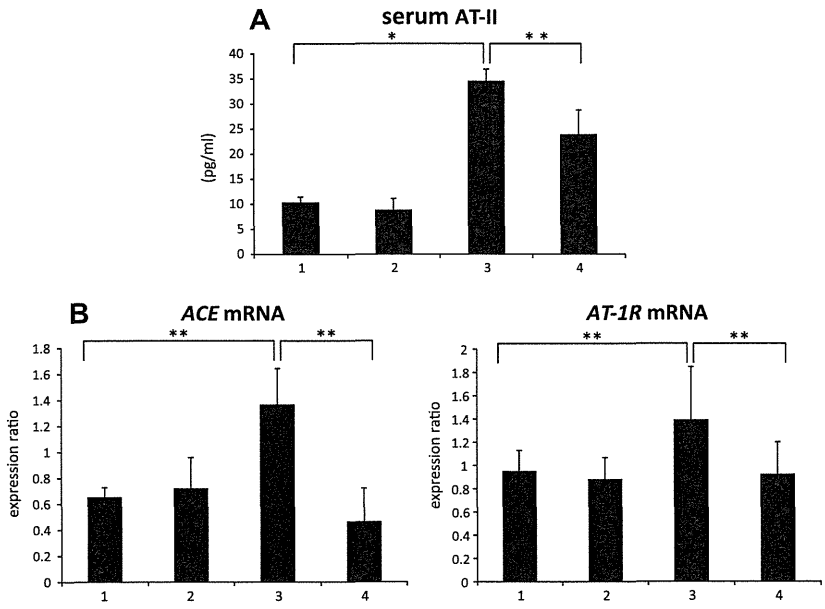

Fig. 3. Effects of EGCG on renin-angiotensin system in the experimental rats. (A) The serum concentrations of AT-II were measured using enzyme immunoassay. (B) The expression levels of ACE and AT-1R mRNA in the livers of the experimental rats were examined by quantitative real-time RT-PCR by using specific primers. The values are expressed as mean ± SD. $^{*}P < 0.001$, $^{**}P < 0.05$.

3.6. Effects of EGCG on serum levels of TNF-α and IL-6 and hepatic expression of TNF-α, IL-6, IL-1β, and MCP-1 mRNA in the experimental rats

Chronic inflammation plays a critical role in the progression of liver fibrosis and subsequent HCC development [5]. Therefore, the levels of inflammatory mediators, including TNF-α, IL-6, IL-1β, and MCP-1, were investigated. The serum levels of TNF-α and IL-6 in SHRSP-ZF rats were significantly elevated relative to those in WKY rats (Fig. 5A; $P < 0.05$). There was also a marked increase in the expression levels of *TNF-α*, *IL-6*, *IL-1β*, and *MCP-1* mRNA in the livers of SHRSP-ZF rats (Fig. 5B; $P < 0.05$). Although EGCG treatment did not significantly affect the serum levels of TNF-α and IL-6 in both SHRSP-ZF and WKY rats (Fig. 5A), the treatment significantly decreased the hepatic expression levels of *TNF-α*, *IL-6*, *IL-1β*, and *MCP-1* mRNA in SHRSP-ZF rats (Fig. 5B, $P < 0.05$).

3.7. Effects of EGCG on serum parameters in the experimental rats

Irrespective of EGCG treatment, the serum levels of AST, ALT, total cholesterol, NEFA, and triglycerides in SHRSP-ZF rats were significantly higher than those in WKY rats (Table 2; $P < 0.05$). The serum levels of glucose and insulin increased significantly, while the value of QUICKI, a useful index of insulin sensitivity [36], decreased ($P < 0.05$). The serum levels of leptin in SHRSP-ZF rats were significantly elevated relative to those in WKY rats, but the levels of adiponectin were lower ($P < 0.05$). Among the parameters elevated in SHRSP-ZF rats, only the serum level of NEFA was significantly suppressed by EGCG treatment ($P < 0.05$). These findings suggest that, in comparison to the improvement of insulin resistance and adipokine imbalance, reduction of oxidative stress and attenuation of inflammation in the liver (Figs. 4 and 5) are more critical mechanisms of EGCG that prevented the early phase of NASH-related liver carcinogenesis in the present study.

4. Discussion

In order to develop an effective strategy for the prevention of NASH-related liver tumorigenesis, there is a critical need to establish an appropriate rodent model that displays the histopathological and pathophysiological characteristics of NASH. The present study provides the first evidence that SHRSP-ZF rats, which present with obesity, diabetes, and hypertension and thus mimic human metabolic syndrome [14,15], more readily develop hepatic preneoplastic lesions, GST-P^{+} foci, than non-obese and normotensive WKY rats when the rats were fed HFD and received CCl_4 injections. The results of the present study clearly indicate that early phase of hepatic tumorigenesis is associated with accelerated steatosis, liver fibrosis, chronic liver damage, presence of insulin resistance, imbalance of adipokines and induction of chronic inflammation and oxidative stress. Because these pathophysiological conditions are critically involved in the progression of NASH and its related liver tumorigenesis [1–5], we propose that our new model using SHRSP-ZF rats might be useful for analyzing the mechanisms of NASH-related liver tumorigenesis and evaluating the efficacy of specific agents that can prevent such tumorigenesis.

One of the limitations in the current study is that we did not observe hepatocellular neoplasms. This might be associated with the duration of the experiment (8 weeks), which was insufficient to develop hepatic tumors. Therefore, future study should recruit longer-term experiments to see that HFD- and CCl_4-treated SHRSP-ZF rats develop hepatocellular neoplasms. Long-term experiments are also useful for evaluating whether the alteration of hepatic gene expression occurred in the present short-term study contribute to the development of hepatocellular neoplasms practically. In addition, it remains unclear whether, not only obesity, but also hypertension actually plays a critical role in the early events of liver carcinogenesis. There are no previous studies that have evaluated the effect of HFD and CCl_4 treatment in hypertensive SHRSP rats as well as in obese ZF rats. Therefore, in order to dissect the effect of hypertension or obesity in liver carcinogenesis,

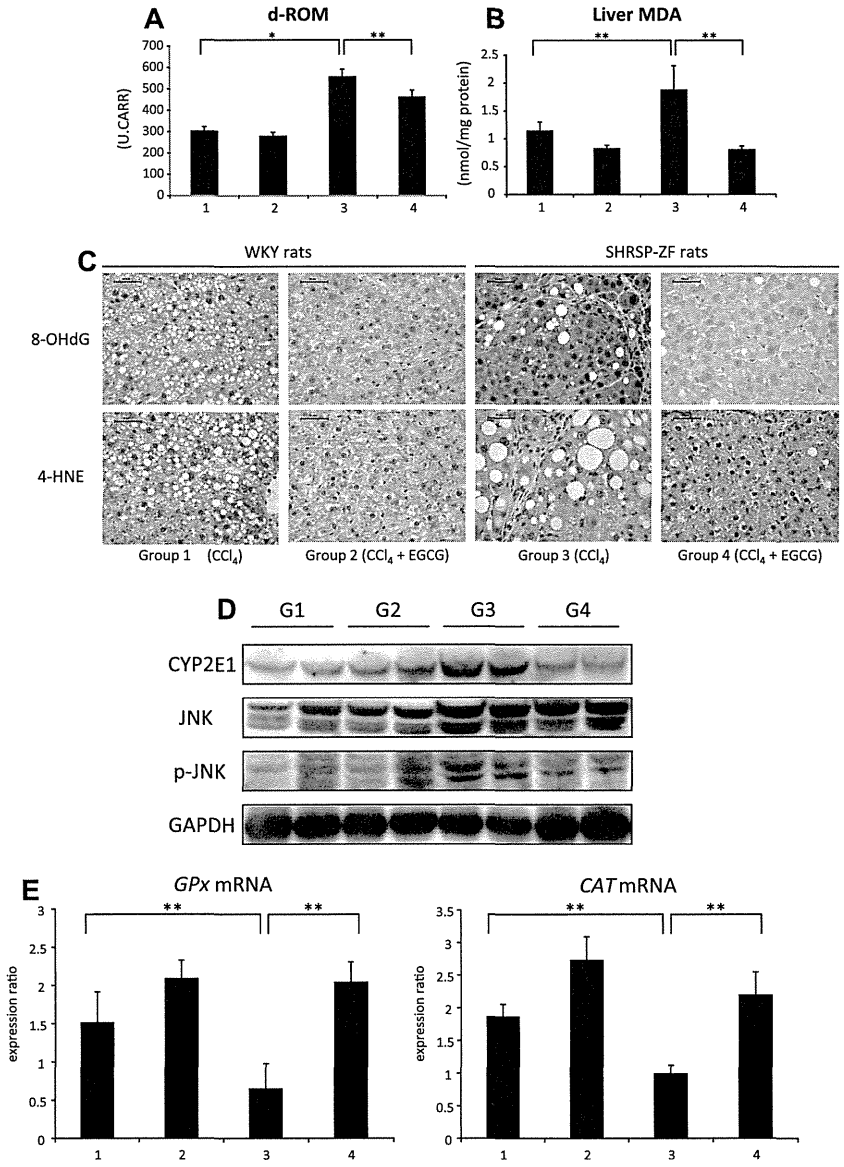

Fig. 4. Effects of EGCG on the serum levels of d-ROM, hepatic concentration of MDA, hepatic expression levels of 8-OHdG, 4-HNE, CYP2E1, JNK, and p-JNK proteins, and hepatic expression levels of GPx and CAT mRNA in the experimental rats. (A) Hydroperoxide levels in the serum were determined by the d-ROM test. (B) The hepatic concentration of MDA was measured by enzyme immunoassay. (C) The results of the immunohistochemical analyses of 8-OHdG and 4-HNE in the livers of the experimental rats. (D) Total proteins were extracted from the livers of the experimental rats and the expression levels of CYP2E1, JNK, and p-JNK proteins were examined by western blot analysis. GAPDH antibody served as the loading control. (E) Total RNA was isolated from the livers of experimental rats, and the expression levels of GPx and CAT mRNA were examined by quantitative real-time RT-PCR by using specific primers. Bars are 50 μm (C). The values are expressed as mean ± SD. $^{*}P < 0.001$, $^{**}P < 0.05$.

additional studies that examine the effects of HFD and CCl_4 treatment in SHRSP rats and ZF rats should be conducted. On the other hand, this study aimed to compare the development of fibrogenesis and preneoplastic lesions (GST-P^+ foci) between the SHRSP-ZF and WKY rats in order to establish NASH-associated liver carcinogenesis. Because GST-P^+ foci are generally accepted as precursor or preneoplastic lesions for HCC in rodents [28,30,37], our findings suggest high susceptibility of the obese and hypertensive SHRSP-ZF rats to hapetocarcinogeneis.

What key mechanism accelerates liver fibrosis and tumorigenesis in SHRSP-ZF rats? We presume that activation of RAS caused by obesity and hypertension is critically involved in such disorders in SHRSP-ZF rats because RAS appears to play a major role in liver fibrosis [38]. AT-II induces the fibrotic effect in activated HSCs by stimulating TGF-β1 expression and increasing collagen synthesis in the liver through the activation of its receptor, AT-1R [8,9,38]. Activated HSCs, which highly express AT-1R, are capable of generating AT-II, suggesting that AT-II can act in an autocrine/paracrine manner in HSCs when liver fibrosis progresses [8]. On the other hand, blocking the generation of AT-II and/or its binding to AT-1R attenuates fibrosis development in experimental rodent models of chronic liver injury [39]. Moreover, the potential beneficial abil-

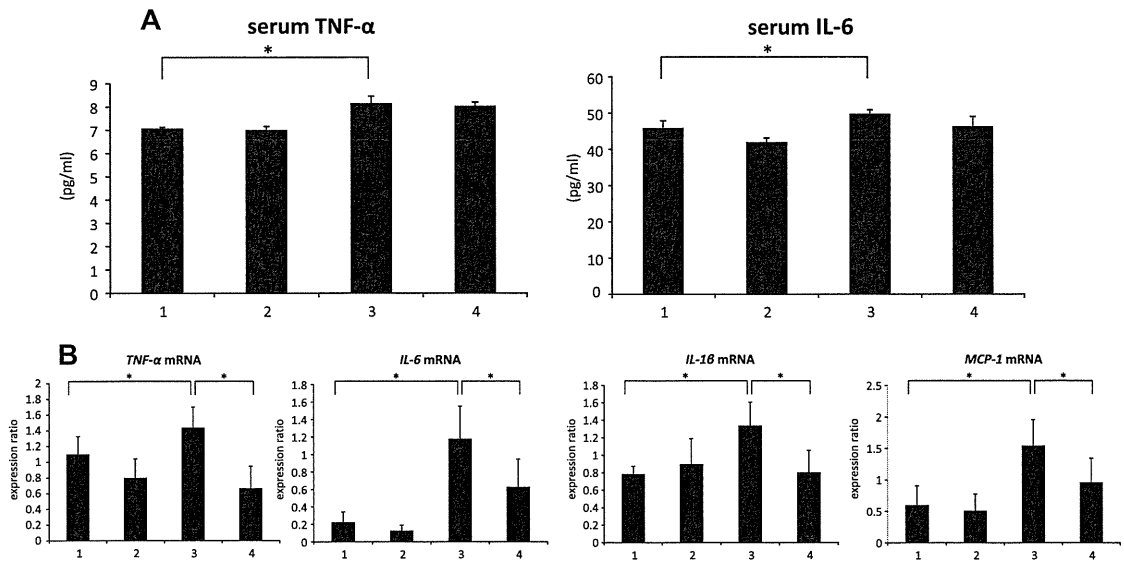

Fig. 5. Effects of EGCG on the serum levels of TNF-α and IL-6 and the expression levels of TNF-α, IL-6, IL-1β, and MCP-1 mRNA in the livers of the experimental rats. (A) The serum concentrations of TNF-α and IL-6 were measured by enzyme immunoassay. (B) Total RNA was isolated from the livers of experimental rats, and the expression levels of TNF-α, IL-6, IL-1β, and MCP-1 mRNA were determined by quantitative real-time RT-PCR by using specific primers. The values are expressed as mean ± SD. $^{*}P < 0.05$.

Table 2
Serum parameters in the experimental rats.

	Group 1	Group 2	Group 3	Group 4
AST (IU/l)	166.8 ± 16.9[a]	140.5 ± 23.6	325.3 ± 45.5[b]	293.0 ± 46.9[c]
ALT (IU/l)	35.5 ± 2.1	36.5 ± 5.4	183.8 ± 42.2[b]	219.3 ± 41.7[c]
Glucose (mg/dl)	106.7 ± 7.2	105.3 ± 4.6	135.1 ± 3.8[b]	127.8 ± 5.3[c]
Insulin (μIU/ml)	25.5 ± 5.4	50.6 ± 8.8	183.4 ± 61.3[b]	223.1 ± 37.5[c]
QUICKI	0.292 ± 0.009	0.269 ± 0.004	0.226 ± 0.008[b]	0.225 ± 0.002[c]
Adiponectin (ng/ml)	52.9 ± 1.9	52.2 ± 0.4	35.2 ± 5.8[b]	35.4 ± 4.0[c]
Leptin (pg/ml)	47.4 ± 4.7	48.4 ± 3.2	400.4 ± 7.3[b]	398.3 ± 5.8[c]
Total cholesterol (mg/dl)	98.2 ± 6.7	93.2 ± 5.0	151.8 ± 9.6[b]	149.8 ± 5.1[c]
NEFA (mEq/L)	0.311 ± 0.038	0.267 ± 0.035	0.698 ± 0.059[b]	0.577 ± 0.046[c,d]
Triglyceride (mg/dl)	53.7 ± 8.1	46.7 ± 8.5	139.9 ± 10.1[b]	128.8 ± 10.9[c]

[a] Mean ± SD.
[b] Significantly different from group 1 by Tukey–Kramer multiple comparison test ($P < 0.05$).
[c] Significantly different from group 2 by Tukey–Kramer multiple comparison test ($P < 0.05$).
[d] Significantly different from group 3 by Tukey–Kramer multiple comparison test ($P < 0.05$).

ity of RAS inhibitors in the attenuation of liver fibrosis in patients with NASH has been shown in clinical trials [40]. Therefore, in the present study, activation of RAS plays a pivotal role in the progression of liver fibrosis in obese and hypertensive SHRSP-ZF rats. EGCG inhibits this fibrogenesis, at least in part, by targeting RAS activation because this agent decreases serum levels of AT-II and suppresses the expression of *ACE* and *AT-1R* mRNA in the liver of these rats. The inhibition of liver fibrosis is significant when considering the chemoprevention of HCC because the risk of liver carcinogenesis increases along with the progression of liver fibrosis [41].

In the liver, RAS is also involved in chronic inflammation and oxidative stress, both of which play a critical role in the progression of fibrosis and subsequent carcinogenesis [8,33]. Administration of AT-II to rats induces HSCs activation, hepatic inflammation, oxidative stress, and lipid peroxidation [42]. Increased systemic AT-II also augments hepatic fibrosis and promotes inflammation and oxidative stress in rats undergoing biliary fibrosis [43]. AT-II stimulates the secretion of inflammatory cytokines such as TNF-α and MCP-1 [44], both of which are involved in the progression of NASH [2], suggesting that targeting RAS might be an effective way to attenuate chronic inflammation and reduce oxidative stress in NASH. AT-1R blockade suppresses HSCs activation, inhibits TNF-α expression, and reduces oxidative stress in rats fed a methionine-choline-deficient diet [39]. The specific delivery of an AT-1R blocker to activated HSCs also reduces inflammation and advanced liver fibrosis in rats [45]. Therefore, consistent with these reports [39,45], EGCG might also prevent liver fibrosis and subsequent tumorigenesis in obese and hypertensive rats by reducing chronic inflammation, systemic oxidative stress, and liver peroxidation, which were induced by RAS activation in the present study. In particular, the effects of EGCG on suppression of the elevated CYP2E1 protein in SHRSP-ZF rats is significant because CYP2E1, which is increased by HFD feeding, is critical in NASH development by promoting oxidative stress, lipid peroxidation, and inflammation [34,35].

Numerous clinical trials have been conducted to develop a therapy that is of proven benefit for NASH; however, no optimal treatment for this disease has yet been found. One of the most practical approaches to treat NASH is targeting insulin resistance and oxidative stress, both of which are implicated as key factors contributing to hepatic injury in patients with NASH [2]. A meta-analysis has

shown that thiazolidinediones, insulin sensitizers regulating glucose metabolism, improve steatosis and serum ALT levels in these patients [46]. In a recent randomized trial with NASH patients, treatment with vitamin E, an antioxidant, also reduced steatosis, lobular inflammation, and serum ALT and AST levels [47]. In the present study, EGCG significantly prevented NASH-related liver fibrosis and tumorigenesis, at least in part, by reducing oxidative stress. Moreover, EGCG also suppresses obesity-related liver and colorectal carcinogenesis by improving hyperinsulinemia [21,23]. The effects of GTCs, whereby they suppress metabolic syndrome, have also been investigated in laboratory animal, epidemiological, and intervention studies [17–19]. These reports [18,19,21,23], together with our findings described here, strongly suggest that GTCs may be useful for preventing the progression of NASH-related liver tumorigenesis, which is associated with oxidative stress and insulin resistance.

Finally, it should be mentioned that the beneficial effects of GTCs have been reported in clinical trials. Supplementation with GTCs can significantly prevent the development of both colorectal adenomas and prostate cancers without causing adverse effects [48,49]. These findings are significant because there are risks associated with medications that are expected to improve NASH, such as weight gain with thiazolidinediones and cardiovascular events and hemorrhagic stokes with vitamin E [46,47]. In summary, our data showed for the first time that liver fibrosis and the development of hepatocellular preneoplastic lesions (GST-P$^+$ foci) are significantly enhanced in obese and hypertensive SHRSP-ZF rats treated with HFD and CCl_4, which have characteristics similar to human NASH. Administration of EGCG effectively prevents liver fibrosis and early stage of hepatocarcinogenesis in these rats by targeting RAS activation and the subsequent inflammation and oxidative stress. Previous rodents studies have shown that GTCs prevent hypertension and target organ damage induced by AT-II through the reduction of oxidative stress [50,51]. GTCs also have a significant inhibitory effect on the activity of ACE and this might be associated with the suppression of high blood pressure in a clinical trial [52]. Although we did not measure the blood pressure of experimental rats in the present study, the results from both experimental and clinical studies [50–52], together with those of present study, strongly indicate the possibility of GTCs, including EGCG, to inhibit RAS activation and to decrease blood pressure subsequently.

In conclusion, our model could be a good option, allowing researchers to study not only the mechanisms involved in NASH-associated hepatocarcinogenesis and the early events involved in tumor formation, but also approaches to HCC prevention in NASH patients focusing on the molecular regulators of the disease. In addition, use of EGCG can improve the NAS score, reduce oxidative stress, and also attenuate chronic inflammation. EGCG therapy represents a potential new strategy for preventing the development of hepatic fibrosis and neoplasm in NASH patients.

5. Conflict of Interest

None declared.

Appendix A. Supplementary material

Supplementary data associated with this article can be found, in the online version, at http://dx.doi.org/10.1016/j.canlet.2013.08.031.

References

[1] A.B. Siegel, A.X. Zhu, Metabolic syndrome and hepatocellular carcinoma: two growing epidemics with a potential link, Cancer 115 (2009) 5651–5661.
[2] D.J. Chiang, M.T. Pritchard, L.E. Nagy, Obesity, diabetes mellitus, and liver fibrosis, Am. J. Physiol. Gastrointest. Liver Physiol. 300 (2011) G697–702.
[3] A.M. Diehl, Hepatic complications of obesity, Gastroenterol. Clin. North Am. 34 (2005) 45–61.
[4] A.P. Rolo, J.S. Teodoro, C.M. Palmeira, Role of oxidative stress in the pathogenesis of nonalcoholic steatohepatitis, Free Radical Biol. Med. 52 (2012) 59–69.
[5] G. Szabo, D. Lippai, Molecular hepatic carcinogenesis: impact of inflammation, Dig. Dis. 30 (2012) 243–248.
[6] B.Q. Starley, C.J. Calcagno, S.A. Harrison, Nonalcoholic fatty liver disease and hepatocellular carcinoma: a weighty connection, Hepatology 51 (2010) 1820–1832.
[7] Y. Nabeshima, S. Tazuma, K. Kanno, H. Hyogo, K. Chayama, Deletion of angiotensin II type I receptor reduces hepatic steatosis, J. Hepatol. 50 (2009) 1226–1235.
[8] R. Bataller, P. Sancho-Bru, P. Gines, D.A. Brenner, Liver fibrogenesis: a new role for the renin-angiotensin system, Antioxid. Redox Signal. 7 (2005) 1346–1355.
[9] E. Matthew Morris, J.A. Fletcher, J.P. Thyfault, R. Scott Rector, The role of angiotensin II in nonalcoholic steatohepatitis, Mol. Cell. Endocrinol. (2012) (Epub ahead of print).
[10] A.D. de Kloet, E.G. Krause, S.C. Woods, The renin angiotensin system and the metabolic syndrome, Physiol. Behav. 100 (2010) 525–534.
[11] K. Yasui, E. Hashimoto, Y. Komorizono, K. Koike, S. Arii, Y. Imai, T. Shima, Y. Kanbara, T. Saibara, T. Mori, S. Kawata, H. Uto, S. Takami, Y. Sumida, T. Takamura, M. Kawanaka, T. Okanoue, Japan NASH Study Group, Characteristics of patients with nonalcoholic steatohepatitis who develop hepatocellular carcinoma, Clin. Gastroenterol. Hepatol. 9 (2011) 428–433.
[12] M. Moreno, L.N. Ramalho, P. Sancho-Bru, M. Ruiz-Ortega, F. Ramalho, J.G. Abraldes, J. Colmenero, M. Dominguez, J. Egido, V. Arroyo, P. Gines, R. Bataller, Atorvastatin attenuates angiotensin II-induced inflammatory actions in the liver, Am. J. Physiol. Gastrointest. Liver Physiol. 296 (2009) G147–156.
[13] Y. Wei, S.E. Clark, J.P. Thyfault, G.M. Uptergrove, W. Li, A.T. Whaley-Connell, C.M. Ferrario, J.R. Sowers, J.A. Ibdah, Oxidative stress-mediated mitochondrial dysfunction contributes to angiotensin II-induced nonalcoholic fatty liver disease in transgenic Ren2 rats, Am. J. Pathol. 174 (2009) 1329–1337.
[14] J. Hiraoka-Yamamoto, Y. Nara, N. Yasui, Y. Onobayashi, S. Tsuchikura, K. Ikeda, Establishment of a new animal model of metabolic syndrome: SHRSP fatty (fa/fa) rats, Clin. Exp. Pharmacol. Physiol. 31 (2004) 107–109.
[15] T. Ueno, H. Takagi, N. Fukuda, A. Takahashi, E.H. Yao, M. Mitsumata, J. Hiraoka-Yamamoto, K. Ikeda, K. Matsumoto, Y. Yamori, Cardiovascular remodeling and metabolic abnormalities in SHRSP.Z-Lepr(fa)/IzmDmcr rats as a new model of metabolic syndrome, Hypertens. Res. 31 (2008) 1021–1031.
[16] T. Kochi, M. Shimizu, T. Ohno, A. Baba, T. Sumi, M. Kubota, Y. Shirakami, H. Tsurumi, T. Tanaka, H. Moriwaki, Enhanced development of azoxymethane-induced colonic preneoplastic lesions in hypertensive rats, Int. J. Mol. Sci. 14 (2013) 14700–14711.
[17] S. Sae-tan, K.A. Grove, J.D. Lambert, Weight control and prevention of metabolic syndrome by green tea, Pharmacol. Res. 64 (2011) 146–154.
[18] K.A. Grove, J.D. Lambert, Laboratory, epidemiological, and human intervention studies show that tea (*Camellia sinensis*) may be useful in the prevention of obesity, J. Nutr. 140 (2010) 446–453.
[19] F. Thielecke, M. Boschmann, The potential role of green tea catechins in the prevention of the metabolic syndrome – a review, Phytochemistry 70 (2009) 11–24.
[20] M. Shimizu, S. Adachi, M. Masuda, O. Kozawa, H. Moriwaki, Cancer chemoprevention with green tea catechins by targeting receptor tyrosine kinases, Mol. Nutr. Food Res. 55 (2011) 832–843.
[21] M. Shimizu, Y. Shirakami, H. Sakai, S. Adachi, K. Hata, Y. Hirose, H. Tsurumi, T. Tanaka, H. Moriwaki, (-)-Epigallocatechin gallate suppresses azoxymethane-induced colonic premalignant lesions in male C57BL/KsJ-db/db mice, Cancer Prev. Res. (Phila.) 1 (2008) 298–304.
[22] Y. Shirakami, M. Shimizu, S. Adachi, H. Sakai, T. Nakagawa, Y. Yasuda, H. Tsurumi, Y. Hara, H. Moriwaki, (-)-Epigallocatechin gallate suppresses the growth of human hepatocellular carcinoma cells by inhibiting activation of the vascular endothelial growth factor-vascular endothelial growth factor receptor axis, Cancer Sci. 100 (2009) 1957–1962.
[23] M. Shimizu, H. Sakai, Y. Shirakami, Y. Yasuda, M. Kubota, D. Terakura, A. Baba, T. Ohno, Y. Hara, T. Tanaka, H. Moriwaki, Preventive effects of (-)-epigallocatechin gallate on diethylnitrosamine-induced liver tumorigenesis in obese and diabetic C57BL/KsJ-db/db mice, Cancer Prev. Res. (Phila.) 4 (2011) 396–403.
[24] T. Ogiso, M. Tatematsu, S. Tamano, H. Tsuda, N. Ito, Comparative effects of carcinogens on the induction of placental glutathione S-transferase-positive liver nodules in a short-term assay and of hepatocellular carcinomas in a long-term assay, Toxicol. Pathol. 13 (1985) 257–265.
[25] Z.Y. Wang, R. Agarwal, D.R. Bickers, H. Mukhtar, Protection against ultraviolet B radiation-induced photocarcinogenesis in hairless mice by green tea polyphenols, Carcinogenesis 12 (1991) 1527–1530.
[26] Y. Yasuda, M. Shimizu, H. Sakai, J. Iwasa, M. Kubota, S. Adachi, Y. Osawa, H. Tsurumi, Y. Hara, H. Moriwaki, (-)-Epigallocatechin gallate prevents carbon tetrachloride-induced rat hepatic fibrosis by inhibiting the expression of the PDGFRbeta and IGF-1R, Chem. Biol. Interact. 182 (2009) 159–164.
[27] D.E. Kleiner, E.M. Brunt, M. Van Natta, C. Behling, M.J. Contos, O.W. Cummings, L.D. Ferrell, Y.C. Liu, M.S. Torbenson, A. Unalp-Arida, M. Yeh, A.J. McCullough, A.J. Sanyal, Nonalcoholic steatohepatitis clinical research, design and

validation of a histological scoring system for nonalcoholic fatty liver disease, Hepatology 41 (2005) 1313–1321.
[28] N. Ando, M. Shimizu, M. Okuno, R. Matsushima-Nishiwaki, H. Tsurumi, T. Tanaka, H. Moriwaki, Expression of retinoid X receptor alpha is decreased in 3′-methyl-4-dimethylaminoazobenzene-induced hepatocellular carcinoma in rats, Oncol. Rep. 18 (2007) 879–884.
[29] D. Terakura, M. Shimizu, J. Iwasa, A. Baba, T. Kochi, T. Ohno, M. Kubota, Y. Shirakami, M. Shiraki, K. Takai, H. Tsurumi, T. Tanaka, H. Moriwaki, Preventive effects of branched-chain amino acid supplementation on the spontaneous development of hepatic preneoplastic lesions in C57BL/KsJ-db/db obese mice, Carcinogenesis 33 (2012) 2499–2506.
[30] F. Kassie, M. Uhl, S. Rabot, B. Grasl-Kraupp, R. Verkerk, M. Kundi, M. Chabicovsky, R. Schulte-Hermann, S. Knasmuller, Chemoprevention of 2-amino-3-methylimidazo[4,5-f]quinoline (IQ)-induced colonic and hepatic preneoplastic lesions in the F344 rat by cruciferous vegetables administered simultaneously with the carcinogen, Carcinogenesis 24 (2003) 255–261.
[31] J. Xiao, Y.P. Ching, E.C. Liong, A.A. Nanji, M.L. Fung, G.L. Tipoe, Garlic-derived S-allylmercaptocysteine is a hepato-protective agent in non-alcoholic fatty liver disease in vivo animal model, Eur. J. Nutr. 52 (2013) (2012) 179–191.
[32] J. Iwasa, M. Shimizu, M. Shiraki, Y. Shirakami, H. Sakai, Y. Terakura, K. Takai, H. Tsurumi, T. Tanaka, H. Moriwaki, Dietary supplementation with branched-chain amino acids suppresses diethylnitrosamine-induced liver tumorigenesis in obese and diabetic C57BL/KsJ-db/db mice, Cancer Sci. 101 (2010) 460–467.
[33] H. Yoshiji, R. Noguchi, Y. Ikenaka, K. Kaji, Y. Aihara, H. Fukui, Impact of renin-angiotensin system in hepatocellular carcinoma, Curr. Cancer Drug Targets 11 (2011) 431–441.
[34] M.A. Abdelmegeed, A. Banerjee, S.H. Yoo, S. Jang, F.J. Gonzalez, B.J. Song, Critical role of cytochrome P450 2E1 (CYP2E1) in the development of high fat-induced non-alcoholic steatohepatitis, J. Hepatol. 57 (2012) 860–866.
[35] Y. Wang, L.M. Ausman, R.M. Russell, A.S. Greenberg, X.D. Wang, Increased apoptosis in high-fat diet-induced nonalcoholic steatohepatitis in rats is associated with c-Jun NH2-terminal kinase activation and elevated proapoptotic Bax, J. Nutr. 138 (2008) 1866–1871.
[36] H. Chen, G. Sullivan, L.Q. Yue, A. Katz, M.J. Quon, QUICKI is a useful index of insulin sensitivity in subjects with hypertension, Am. J. Physiol. Endocrinol. Metab. 284 (2003) E804–812.
[37] H. Tsuda, S. Fukushima, H. Wanibuchi, K. Morimura, D. Nakae, K. Imaida, M. Tatematsu, M. Hirose, K. Wakabayashi, M.A. Moore, Value of GST-P positive preneoplastic hepatic foci in dose-response studies of hepatocarcinogenesis: evidence for practical thresholds with both genotoxic and nongenotoxic carcinogens. A review of recent work, Toxicol. Pathol. 31 (2003) 80–86.
[38] Y. Nabeshima, S. Tazuma, K. Kanno, H. Hyogo, M. Iwai, M. Horiuchi, K. Chayama, Anti-fibrogenic function of angiotensin II type 2 receptor in CCl4-induced liver fibrosis, Biochem. Biophys. Res. Commun. 346 (2006) 658–664.
[39] A. Hirose, M. Ono, T. Saibara, Y. Nozaki, K. Masuda, A. Yoshioka, M. Takahashi, N. Akisawa, S. Iwasaki, J.A. Oben, S. Onishi, Angiotensin II type 1 receptor blocker inhibits fibrosis in rat nonalcoholic steatohepatitis, Hepatology 45 (2007) 1375–1381.
[40] S. Yokohama, M. Yoneda, M. Haneda, S. Okamoto, M. Okada, K. Aso, T. Hasegawa, Y. Tokusashi, N. Miyokawa, K. Nakamura, Therapeutic efficacy of an angiotensin II receptor antagonist in patients with nonalcoholic steatohepatitis, Hepatology 40 (2004) 1222–1225.
[41] I. Sakaida, K. Hironaka, K. Uchida, C. Suzuki, K. Kayano, K. Okita, Fibrosis accelerates the development of enzyme-altered lesions in the rat liver, Hepatology 28 (1998) 1247–1252.
[42] R. Bataller, E. Gabele, R. Schoonhoven, T. Morris, M. Lehnert, L. Yang, D.A. Brenner, R.A. Rippe, Prolonged infusion of angiotensin II into normal rats induces stellate cell activation and proinflammatory events in liver, Am. J. Physiol. Gastrointest. Liver Physiol. 285 (2003) G642–651.
[43] R. Bataller, E. Gabele, C.J. Parsons, T. Morris, L. Yang, R. Schoonhoven, D.A. Brenner, R.A. Rippe, Systemic infusion of angiotensin II exacerbates liver fibrosis in bile duct-ligated rats, Hepatology 41 (2005) 1046–1055.
[44] R.M. Pereira, R.A. dos Santos, F.L. da Costa Dias, M.M. Teixeira, A.C. Simoes e Silva, Renin-angiotensin system in the pathogenesis of liver fibrosis, World J. Gastroenterol. 15 (2009) 2579–2586.
[45] M. Moreno, T. Gonzalo, R.J. Kok, P. Sancho-Bru, M. van Beuge, J. Swart, J. Prakash, K. Temming, C. Fondevila, L. Beljaars, M. Lacombe, P. van der Hoeven, V. Arroyo, K. Poelstra, D.A. Brenner, P. Gines, R. Bataller, Reduction of advanced liver fibrosis by short-term targeted delivery of an angiotensin receptor blocker to hepatic stellate cells in rats, Hepatology 51 (2010) 942–952.
[46] M.O. Rakoski, A.G. Singal, M.A. Rogers, H. Conjeevaram, Meta-analysis: insulin sensitizers for the treatment of non-alcoholic steatohepatitis, Aliment. Pharmacol. Ther. 32 (2010) 1211–1221.
[47] A.J. Sanyal, N. Chalasani, K.V. Kowdley, A. McCullough, A.M. Diehl, N.M. Bass, B.A. Neuschwander-Tetri, J.E. Lavine, J. Tonascia, A. Unalp, M. Van Natta, J. Clark, E.M. Brunt, D.E. Kleiner, J.H. Hoofnagle, P.R. Robuck, NASH CRN, Pioglitazone, vitamin E, or placebo for nonalcoholic steatohepatitis, N. Engl. J. Med. 362 (2010) 1675–1685.
[48] M. Shimizu, Y. Fukutomi, M. Ninomiya, K. Nagura, T. Kato, H. Araki, M. Suganuma, H. Fujiki, H. Moriwaki, Green tea extracts for the prevention of metachronous colorectal adenomas: a pilot study, Cancer Epidemiol. Biomarkers Prev. 17 (2008) 3020–3025.
[49] S. Bettuzzi, M. Brausi, F. Rizzi, G. Castagnetti, G. Peracchia, A. Corti, Chemoprevention of human prostate cancer by oral administration of green tea catechins in volunteers with high-grade prostate intraepithelial neoplasia: a preliminary report from a one-year proof-of-principle study, Cancer Res. 66 (2006) 1234–1240.
[50] M. Antonello, D. Montemurro, M. Bolognesi, M. Di Pascoli, A. Piva, F. Grego, D. Sticchi, L. Giuliani, S. Garbisa, G.P. Rossi, Prevention of hypertension, cardiovascular damage and endothelial dysfunction with green tea extracts, Am. J. Hypertens. 20 (2007) 1321–1328.
[51] I. Papparella, G. Ceolotto, D. Montemurro, M. Antonello, S. Garbisa, G. Rossi, A. Semplicini, Green tea attenuates angiotensin II-induced cardiac hypertrophy in rats by modulating reactive oxygen species production and the Src/epidermal growth factor receptor/Akt signaling pathway, J. Nutr. 138 (2008) 1596–1601.
[52] I. Kurita, M. Maeda-Yamamoto, H. Tachibana, M. Kamei, Antihypertensive effect of Benifuuki tea containing O-methylated EGCG, J. Agric. Food Chem. 58 (2010) 1903–1908.

Hepatology Research

Hepatology Research 2013; 43: 106–112 doi: 10.1111/hepr.12004

Special Report

Nutritional status and quality of life in current patients with liver cirrhosis as assessed in 2007–2011

Makoto Shiraki,[1] Shuhei Nishiguchi,[2] Masaki Saito,[2] Yoshitaka Fukuzawa,[3] Toshihiko Mizuta,[4] Masaki Kaibori,[5] Tatsunori Hanai,[1] Kayoko Nishimura,[6] Masahito Shimizu,[1] Hisashi Tsurumi[1] and Hisataka Moriwaki[1]

[1]*The First Department of Internal Medicine, Gifu University School of Medicine, Gifu,* [2]*Division of Hepatobiliary and Pancreatic Disease, Department of Internal Medicine, Hyogo College of Medicine, Hyogo,* [3]*Medical Education Center, Aichi Medical University School of Medicine, Aichi,* [4]*Department of Internal Medicine, Saga Medical School, Saga University, Saga,* [5]*Department of Surgery, Kansai Medical University, Osaka, and* [6]*Center for Nutrition Support and Infection Control, Gifu University Hospital, Gifu, Japan*

Aim: Current guidelines recommended adequate nutritional support for patients with liver cirrhosis to improve clinical outcome and quality of life (QOL). However, these evidences were obtained more than 10 years ago when malnutrition prevailed. In recent years, the impact of obesity on liver damage and carcinogenesis has grown. We attempted to elucidate the nutritional state and QOL in present cirrhotics.

Methods: A research group supported by the Ministry of Health, Labor and Welfare of Japan recruited 294 cirrhotics between 2007 and 2011. Subjects comprised 171 males and 123 females, 158 of whom had hepatocellular carcinoma (HCC) and Child–Pugh grades A : B : C were 154:91:49. Anthropometry, blood biochemistry and indirect calorimetry were conducted, and QOL was measured using Short Form-8.

Results: The mean body mass index (BMI) of all patients was 23.1 ± 3.4 kg/m^2, and 31% showed obesity (BMI ≥ 25.0). In subjects without ascites, edema or HCC, mean BMI was 23.6 ± 3.6, and 34% had obesity. Protein malnutrition defined as serum albumin of less than 3.5 g/dL and energy malnutrition as respiratory quotient of less than 0.85 appeared in 61% and 43%, respectively, and protein-energy malnutrition (PEM) in 27% of all subjects. Among subjects without HCC, each proportion was 67%, 48% and 30%, respectively. QOL was significantly lower on all subscales than Japanese national standard values, but was similar regardless the presence or absence of HCC.

Conclusion: While PEM is still present in liver cirrhosis, an equal proportion has obesity in recent patients. Thus, in addition to guidelines for PEM, establishment of nutrition and exercise guidelines seems essential for obese patients with liver cirrhosis.

Key words: body mass index, energy malnutrition, liver cirrhosis, protein malnutrition, quality of life

INTRODUCTION

BECAUSE THE LIVER plays the central role in nutrient and fuel metabolism, protein-energy malnutrition (PEM) is common in patients with liver cirrhosis.[1,2] Moreover, such malnutrition leads to poor prognosis and decline in the quality of life (QOL) of cirrhotics.[3,4]

Branched-chain amino acid (BCAA) administration for protein malnutrition raises the serum albumin level and improves the QOL and survival of patients with liver cirrhosis.[5–8] Treatment with late-evening snack (LES) for energy malnutrition improves respiratory quotient (RQ), liver dysfunction and QOL.[9,10]

Therefore, the guidelines for the treatment of liver cirrhosis by Japanese Society of Gastroenterology,[11] American Society for Parenteral and Enteral Nutrition[12] and European Society for Clinical Nutrition and Metabolism[13] recommend such nutritional therapy.

However, these evidences were obtained in the cirrhotic patients recruited from 1995–2000, where protein or energy malnutrition prevailed in 50–87%.[1–4] In contrast, in the next 10 years, obesity rate in the cirrhotic patients rose to approximately 30%.[14] More recently, non-alcoholic steatohepatitis (NASH) or the

Correspondence: Dr Makoto Shiraki, The First Department of Internal Medicine, Gifu University School of Medicine, 1-1 Yanagido, Gifu 501-1194, Japan. Email: mshiraki-gif@umin.ac.jp
Received 11 August 2012; revision 7 October 2012; accepted 15 October 2012.